SCHOOL OF ENGINEERING
OLD DOMINION UNIVERSITY
NORFOLK, VIRGINIA

ANALYTICAL AND NUMERICAL INVESTIGATION OF STRUCTURAL RESPONSE OF COMPLIANT WALL MATERIALS
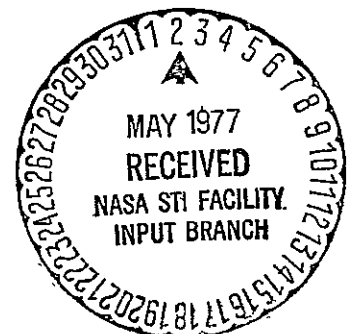
By

R. Balasubramanian

G.L. Goglia, Principal Investigator

Final Report (Supplement No. 1)

Prepared for the
National Aeronautics and Space Administration
Langley Research Center
Hampton, Virginia

April 1977

SCHOOL OF ENGINEERING
OLD DOMINION UNIVERSITY
NORFOLK, VIRGINIA

ANALYTICAL AND NUMERICAL INVESTIGATION OF STRUCTURAL RESPONSE OF COMPLIANT WALL MATERIALS

By

R. Balasubramanian

G.L. Goglia, Principal Investigator

Final Report (Supplement No. 1)

April 1977

TABLE OF CONTENTS -

TABLE OF CONTENTS - CONCLUDED

LIST OF FIGURES

(cont'd.)

iii

LIST OF FIGURES - CONCLUDED

LIST OF TABLES

ANALYTICAL AND NUMERICAL INVESTIGATION OF STRUCTURAL
RESPONSE OF COMPLIANT WALL MATERIALS

By

R. Balasubramanian[1]

SUMMARY

Surface motion of compliant walls in drag reduction experiments has been
analyzed. Critical comparison is made between the dynamic motion of the structure
and the postulated mechanism of drag reduction (ref. 1). The spectrum of surface
motion indicates that membranes over deep cavities respond at low frequencies
and large wavelengths. The membrane over a deep cavity is therefore found not
to yield the desired response predicted by the postulated mechanism. The mem-
brane over a thin air gap is found to act as a wavelength chopper, and analysis
of the nonlinear response of that compliant surface indicates its possible
suitability for compliant wall experiments. Periodic structures are found to
lock in the desired wavelengths of motion, and it is found that at least in
Kramer's (ref. 2) initial experiments they could have produced high frequency
surface motions. Laminated structures are found to be very ineffective as com-
pliant models, except when there is no bonding between the membrane and the
backing. Computer programs developed for these analyses are documented in this
report.

INTRODUCTION

The impetus for the compliant wall drag reduction program at NASA-Langley
Research Center, came mainly from the fact that reduction in turbulent skin friction
drag reported in the literature (refs. 2 to 5) may be translated into potentially

---

[1] Research Associate, School of Engineering, Old Dominion University,
Norfolk, Virginia 23508.

large savings in energy for CTOL aircraft. The group effort at Langley was initiated with the goals of:

1. Understanding the conditions, if any, for favorable compliant motions,

2. Duplicating previous data under rigorously controlled test conditions, and

3. Designing improved experiments to further understanding of the compliant wall drag reduction phenomenon.

The present work under NSG 1236 eminated from a desire to evaluate the structural response of compliant walls in successful drag reduction experiments.

THE PROPOSED FLUID-STRUCTURE INTERACTION MODEL

Bushnell (ref. 1) has proposed a compliant wall interaction model by which a fully turbulent flow over a vibrating compliant wall could produce reduced skin friction on the wall. In the past few years, researchers have developed an understanding of some details of the streaky flow adjacent to a rigid wall. The proposed mechanism of Bushnell (ref. 1) suggests that the induced aerodynamic pressure field due to the structural motion could impose a high frequency stabilizing modulation of the "preburst" flow and thereby reducing the rate of production of turbulent shear. Numerical experiments by Orszag (ref. 6) and active wall experiments reported by Kendall and Collins (ref. 7) suggest that such a mechanism may well be valid.

Based on this model, the favorable structural motion has a wavelength on the order of $\lambda^+ = 100$, in wall units, [$\lambda = \lambda^+ \nu/(\sqrt{C_f/2}\ U_\infty)$; where C_F is the skin friction coefficient, ν is the kinematic viscosity, and U_∞ is the mean flow velocity], a wave speed $\tilde{C} = 0.3\ U_\infty$, and an amplitude $a^+ \approx 0(1.0)$. For low speed air experiments, this criterion indicates that the drag reduction effect can only be observed in compliant walls made of elastomers and carefully designed to obtain the desired wavemotions under given flow conditions. Indeed, most of the reported "successful" experiments were in compliant walls using thin membranes.

According to the proposed model, for a flow speed of 70 ft/sec (21.34 m/sec), the structural motion favorable to a compliant effect has a wavelength

of 0.066 ins. (1.68 mm)., an amplitude of .660 µins. (16.76 µm),. and a frequency of 3700 Hz.

THE EXPERIMENTAL PROGRAM AT. LANGLEY. RESEARCH CENTER

The compliant wall experiments conducted by the Fluid Mechanics Branch, High Speed Aircraft Division of Langley Research Center can be classified into two categories of test conditions: (1) Wind tunnel test conducted in a Low Turbulence Pressure Tunnel (LTPT) with flow speeds of 210 ft/sec (64 m/sec) and higher. The results of these experiments have been reported (ref. 5). (2) Tests conducted in a 7 in. by 11 in. low speed tunnel where flow speeds can be varied between 50 and 150 ft/sec (15.2 to 45.7 m/sec).

Because of the differences in test conditions, model geometries are scaled differently for these experiments. So far, LTPT tests have been made in laminated structures only and the 7 in. by 11 in. tunnel tests have been done on a wide variety of models.

Currently, drag measurements are made using a direct drag balance, and facilities for monitoring surface motions during an actual run are available. Thus, in some cases, comparison between the theoretical data presented in this report and the experimental values has been possible.

OVERALL PERSPECTIVE OF THE STRUCTURAL ANALYSIS PROGRAM
RELATED TO COMPLIANT WALL EXPERIMENTS

Material Requirements

The compliant surfaces used for testing have been built of elastomers. The manufacturer's quoted properties of the various film materials as well as the foam substrate are often an unreliable guide to the true conditions in the stock material. The compliant wall materials used in the Langley experiments were therefore carefully tested in the Materials Division of Langley Research Center. Materials were tested in film foam on an Eustron model TTC tensile testing machine. Typical compliant materials used in the experiments were PVC plastisol, Alathon, latex rubber, aluminized PVC, polyethylene and aluminized mylar. A brief summary of materal testing is reported elsewhere (see Appendix A).

Structural Response Analysis

Previous investigations of compliant wall structural interaction (refs. 8, 9, 10) have been based on speculation that the compliance of the structure acts as a stabilizer of the transitional instability. Neither the effect of supports nor the presence of nonlinear effects in the motion received any attention in these works. In some later works (ref. 11) the viscoelastic nature of the material has been included in the analysis. However, the problem of fluid-structural interaction has largely been given only cursory attention.

The present work has attempted to remedy this situation in two directions:

1. Modelling of the actual structure has been done carefully; wherever numerical simulations are appropriate they have been used. When semi-analytic methods are useful we have employed these. Identification of the various loads acting on the structure under test conditions is another major problem given attention in this report.

2. Inclusion of structural nonlinearities or other gross effects which can affect the actual motion has been made after proper evaluation (for instance, if the loading is moderately small, structural nonlinearity need not be included when the nonlinear effects are mainly geometric). If acoustic effects are important these effects need to be included in the analysis. If mean flow effects come into the picture (flutter, divergence) then the appropriate loading due to this needs to be included.

Because of the wide variety of compliant models, we resorted to a classification which covers basically most of the compliant experiments reported in the literature:

1. Laminated structures: Usually membranes bonded to substrates which are rigidly fixed at the bottom. The membranes may be under tension;

2. Membranes under deep cavities: The cavities could be fluid filled;

3. Membranes under narrow air gaps; and

4. Periodic structures: The periodicity due to multiplicity of equally spaced supports usually in the flow direction.

STRUCTURAL OSCILLATIONS IN THE PRESENCE OF FLOW

The response of a structure to loading in the presence of a fluid is quite different from its in vacuo response. The motion of the structure introduces a disturbance field in the fluid which itself is felt by the structure. Thus there are two distinct boundary value problems that need to be solved:

1. The boundary value problem of the structure of volume V, with the given dynamic loads external to it and body forces: only a part of its total boundary surface S --say, S_1 --interacts with the fluid.

2. A boundary value problem for a fluid region R interacting with the elastic body, the solution of which has the form

$$p = p(\overline{U}, x) \tag{1}$$

where p is the hydrodynamic pressure at the point X on S_1 and $\overline{U}$ is the displacement of the points of the body on the boundary.

We thus break up the total loading acting on the structure into three components:

a. P^e, the external pressure loading acting on the structure causing the initial or primary motion.

b. P^i, the induced pressure loading on the structure due to its interaction with the primary fluid.

c. P^b, the back pressure or the induced pressure from the back side of of the structure.

External Force Field

For compliant wall experiments under consideration in this report, the external pressure loading P^e can be broken down into three components:

1. A random convected pressure load due to the turbulent boundary layer. (The pressure pulses travel at speeds between 0.5 to 0.8 times free stream velocity.) Bull (ref. 12) has made measurements of the spectral pattern of this pressure for subsonic flows. At lowest wave numbers, Bull's spectrum

does not drop off, and we have used the dropoff suggested by Von Karmen and Lin (ref. 13), i.e., $E(k,t) = F(I,\varepsilon^o,k,t)$ where ε is the eddy diffusivity, and I is Loitsianskii's integral.

Wherever only qualitative trends are desired (e.g., expected value of surface amplitude, power spectral response) we have used Bull's spectrum (with the proper modifications) for analysis.

Recently, we have developed a full simulation of the random pressure field using Monte Carlo techniques (ref. 14). In some analyses using numerical simulation for structural response (specifically membranes under thin air gaps, laminated structures using NASTRAN), we have used the simulated pressure field. In figures 1 and 2 we display the modified wall pressure spectrum and the simulated wall pressure history at points for a low speed turbulent boundary layer.

2. Static pressure differentials. In some wind tunnels there will be a difference between the static pressure of the fluid and the ambient pressure, which will be a function of the flow speed. A knowledge of this deviation is essential since it can cause primary surface deformations.

3. Pressure gradients. The presence of a static pressure gradient in the tunnel affects the theoretical predictions in two ways. In all of the analyses presented here, a tacit assumption is made that the mean flow is parallel shear flow. The nonparallel effect due to gradients requires a nonparallel stability model for the proposed model (ref. 1). Furthermore, the induced pressure force evaluation also suffers from lack of consideration of the nonparallelness. Hence, if pressure gradients are present in a given experiment, we shall ignore that experiment altogether.

Induced Pressure Field P^i

The motion of the structure introduces a perturbation pressure field into the flow and hence on itself. Sophisticated fluid theories can be developed to evaluate the boundary value problem of a flow of infinite extent--one boundary of which changes with time. Since many of the experiments were conducted in the predivergence regime we have accepted a lower order theory, viz. piston theory (potential flow model), for developing the expression for induced pressure on the structure.

6
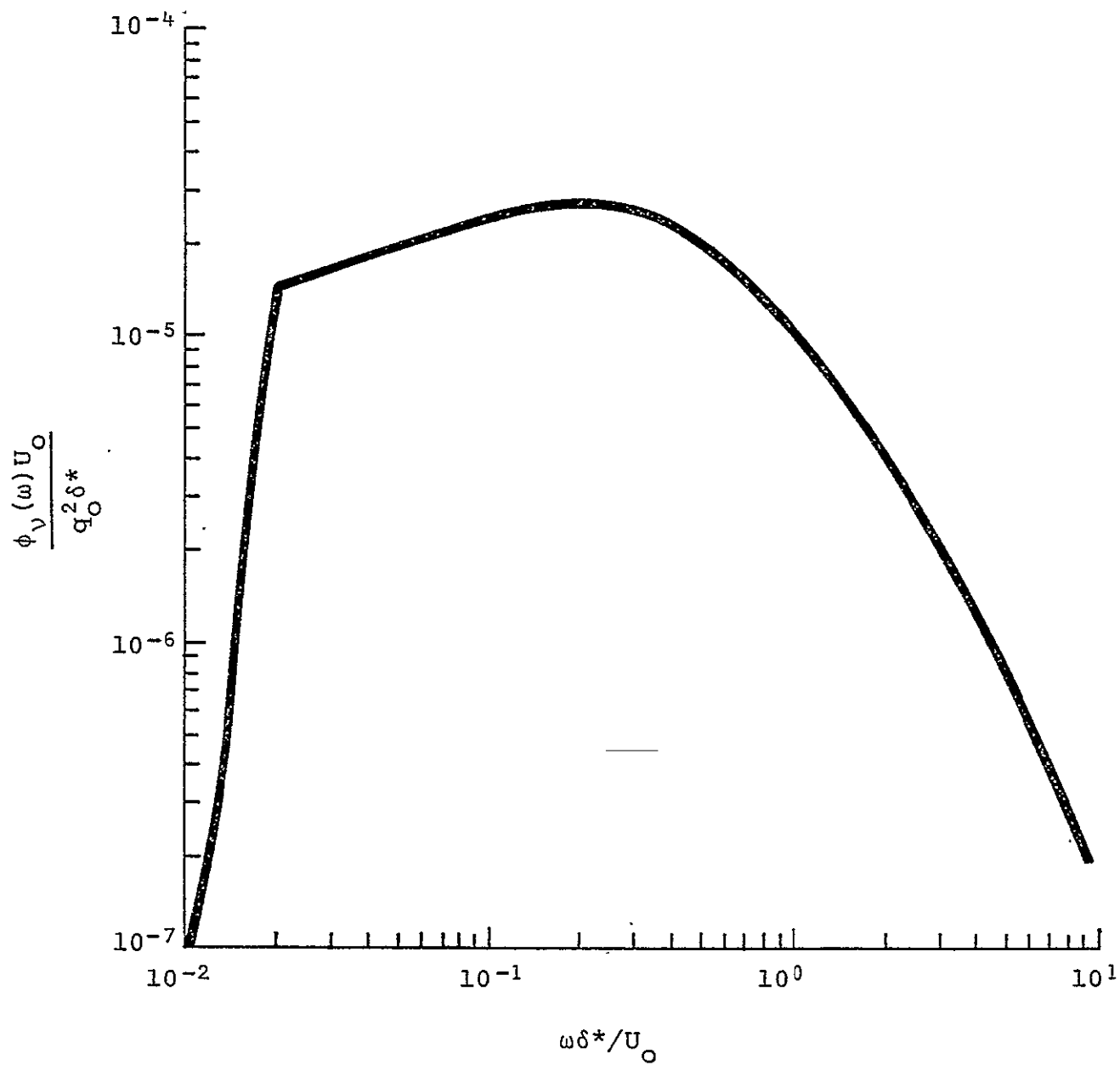
Figure 1. Modified pressure spectrum for subsonic flows used for analysis.
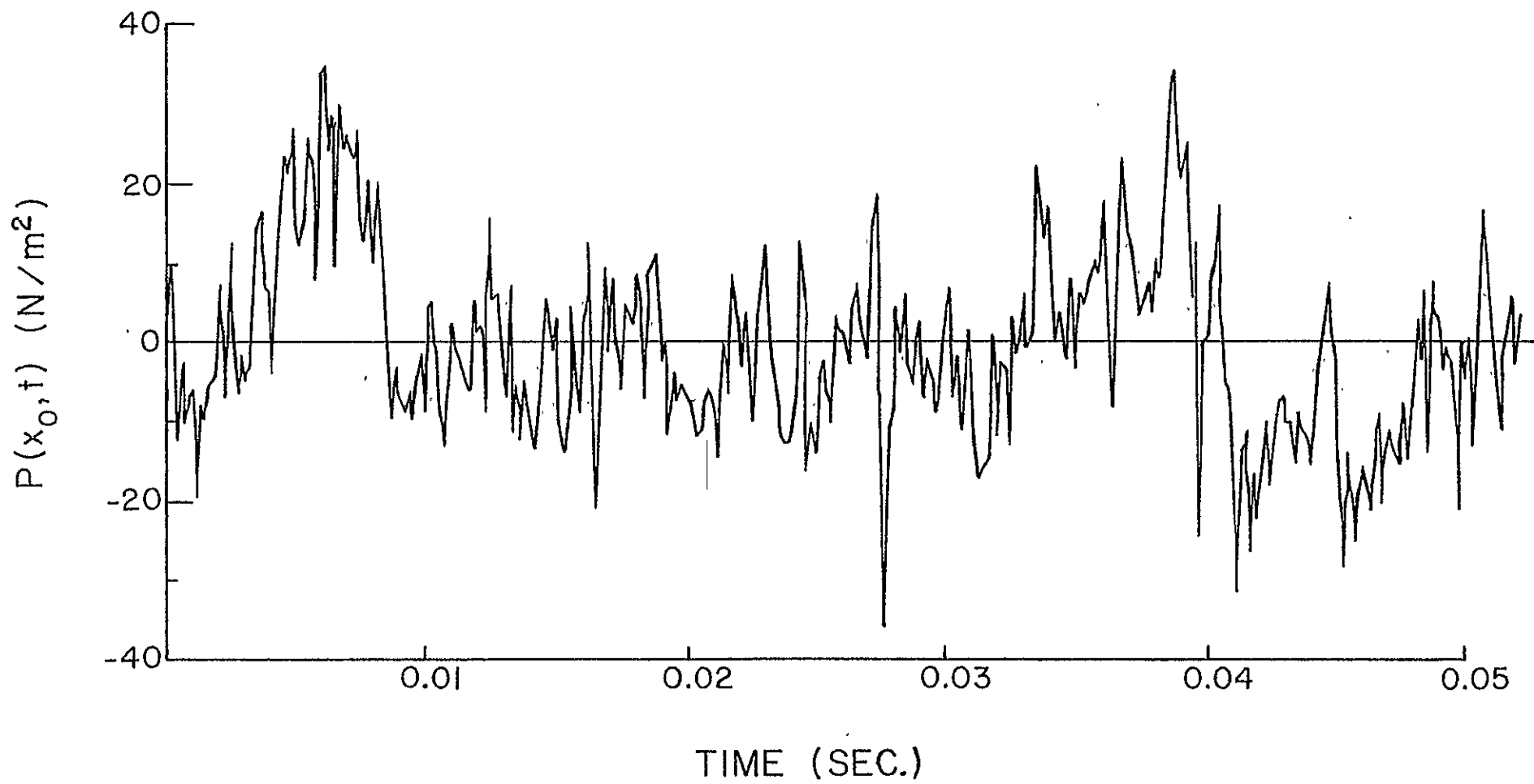
Figure 2. Simulated wall pressure history using Monte Carlo technique (ref. 14).

The inclusion of the induced pressure field is unwarranted in some cases. These are cases where the divergence speed of the model is far above the operating speed. An analysis which neglected these forces would still yield accurate results for structural response in these cases. As we proceed in these analyses we shall indicate the inclusion (or otherwise) for different experiments justifying our reasons for same.

<div align="center">Back Pressure P^b</div>

Some of the models tested contained fluid filled cavities beneath them. We shall develop theoretical expressions for evaluating these in the next sections.

<div align="center">ANALYSIS OF A MEMBRANE OVER A DEEP CAVITY WITH EXTERNAL
FLOW OVER THE MEMBRANE</div>

We consider (fig. 3) a membrane of flexural rigidity. D, tension T, simply supported on ends $x = 0$, $x = a$, and $y = 0$ and $y = b$, and of thickness h and density ζ.
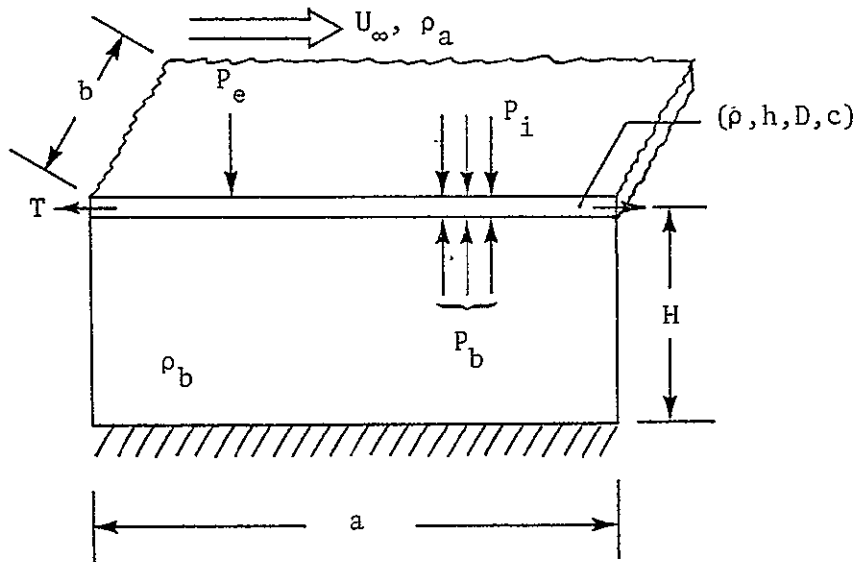
<div align="center">Figure 3. Membrane over a deep cavity.</div>

The dynamic equation of motion for this membrane is given by

$$\rho h \frac{\partial^2 w}{\partial t^2} + C \frac{\partial w}{\partial t} \mp D\nabla^2\nabla^2 w - T\nabla^2 w = P^e + P^i + P^b \tag{2}$$

In equation (2) we have neglected effects of midplane stretching. When non-linear (stretching) effects need to be taken into consideration, we use the following equations:

$$\rho h \frac{\partial^2 w}{\partial t^2} + C \frac{\partial w}{\partial t} + D\nabla^4 w - \left(N_x \frac{\partial^2 w}{\partial x^2} + N_y \frac{\partial^2 w}{\partial y^2} + N_{xy} \frac{\partial^2 w}{\partial x \partial y} \right) = P^e + P^i + P^b \tag{3}$$

$$\rho h \frac{\partial^2 u}{\partial t^2} + C \frac{\partial u}{\partial t} + \left(\frac{Eh}{1 - \nu^2} \right) \left\{ \frac{\partial^2 u}{\partial x^2} + \left(\frac{1 - \nu}{2} \right) \frac{\partial^2 u}{\partial y^2} + \left(\frac{1 + \nu}{2} \right) \frac{\partial^2 v}{\partial x \partial y} \right.$$

$$\left. + \frac{\partial w}{\partial x} \left(\frac{\partial^2 w}{\partial x^2} + \left(\frac{1 - \nu}{2} \right) \frac{\partial^2 w}{\partial y^2} \right) + \frac{1 + \nu}{2} \frac{\partial^2 w}{\partial x \partial y} \frac{\partial w}{\partial y} \right\} = 0 \tag{4}$$

and

$$\rho h \frac{\partial^2 v}{\partial t^2} + C \frac{\partial v}{\partial t} + \left(\frac{Eh}{1 - \nu^2} \right) \left\{ \frac{\partial^2 v}{\partial y^2} + \left(\frac{1 - \nu}{2} \right) \frac{\partial^2 v}{\partial x^2} + \frac{1 + \nu}{2} \frac{\partial^2 u}{\partial x \partial y} \right.$$

$$\left. + \frac{\partial w}{\partial y} \left(\frac{\partial^2 w}{\partial y^2} + \frac{1 - \nu}{2} \frac{\partial^2 w}{\partial x^2} \right) + \frac{1 + \nu}{2} \frac{\partial^2 w}{\partial x \partial y} \frac{\partial w}{\partial x} \right\} = 0 \tag{5}$$

and

$$N_x = \left(\frac{Eh}{1 - \nu^2} \right) \left\{ \left(\frac{\partial^2 u}{\partial x^2} + \nu \frac{\partial^2 v}{\partial y^2} \right) + \frac{1}{2} \left[\left(\frac{\partial w}{\partial x} \right)^2 + \nu \left(\frac{\partial w}{\partial y} \right)^2 \right] \right\} \tag{6a}$$

$$N_y = \left(\frac{Eh}{1 - \nu^2} \right) \left\{ \left(\frac{\partial^2 v}{\partial y^2} + \nu \frac{\partial^2 u}{\partial x^2} \right) + \frac{1}{2} \left[\left(\frac{\partial w}{\partial y} \right)^2 + \nu \left(\frac{\partial w}{\partial x} \right)^2 \right] \right\} \tag{6b}$$

$$N_{xy} = \frac{Eh}{2(1 + \nu)} \left\{ \frac{\partial u}{\partial y} + \frac{\partial v}{\partial x} + \frac{\partial w}{\partial x} \frac{\partial w}{\partial y} \right\} \tag{6c}$$

10

Linear Model

We shall assume that the surface motion is made of normal modes in space and has the form

$$w = \sum_{m}^{\infty} \sum_{n}^{\infty} W_{mn}(t) \sin \frac{m\pi x}{a} \sin \frac{n\pi y}{b} \tag{7}$$

Furthermore, we assume that a harmonic dependence on time exists, i.e.,

$$W_{mn}(t) = a_{mn} e^{i\omega t} \tag{8}$$

For the linear problem at hand, equation (8) is a justifiable assumption as long as P^e can be broken down into its harmonic components, i.e.,

$$P^e = \sum_{j} P_j e^{i\omega_j t} .$$

Evaluation of the Back Pressure

Under the assumption that the fluid motion in the cavity is a perturbed state of motion and is irrotational, we define expansions for the velocity potential and the elevation of the surface S_1 as

$$\left. \begin{array}{l} \phi = \epsilon \, \phi^{(1)} + \epsilon^2 \, \phi^{(2)} + \ldots \\ \\ z = z^{(0)} + \epsilon \, z^{(1)} + \ldots \end{array} \right\} \tag{9}$$

$\phi^{(k)}$ satisfies the wave equation

$$\frac{1}{c^2} \frac{\partial^2 \phi^{(k)}}{\partial t^2} = \nabla^2 \phi^{(k)} \tag{10}$$

where c is the speed of sound in the medium.

The boundary conditions are, at η, i.e., on S_1

$$[\eta = z - w(x,y,t)]$$

$$\frac{d\eta}{dt} \equiv 0 = \frac{\partial w}{\partial t} + \frac{\partial \phi}{\partial x}\frac{\partial w}{\partial x} + \frac{\partial \phi}{\partial y}\frac{\partial w}{\partial y} - \frac{\partial \phi}{\partial z} \qquad (11)$$

and at $z = H$

$$\frac{\partial \phi}{\partial n} = 0 \quad , \qquad\qquad \text{i.e.,} \quad \frac{\partial \phi}{\partial z} = 0 \qquad (12)$$

Applying the expansion, equation (9) into equation (11):

$$\frac{\partial z^{(0)}}{\partial t} = 0$$

$$\frac{\partial z^{(1)}}{\partial t} = \frac{\partial \phi^{(1)}}{\partial z} \quad ,$$

yielding

$$z^{(0)} = \text{constant} = 0 \quad ,$$

and since $\sqrt{z^{(0)} + \epsilon\, z^{(1)}} = w$,

$$\frac{\partial w}{\partial t} = \frac{\partial \phi}{\partial z}\,\bigg|_{z=0} \qquad (13)$$

Let us now assume that the solution of equation (10) with the boundary conditions [eqs. (11) and (12)] has the form

$$\phi = a(z)\, a_{mn}(t)\, \sin\frac{m\pi x}{a}\, \sin\frac{n\pi y}{b} \qquad (14)$$

12

Thus

$$a''(z) - \left\{ \left(\frac{m\pi}{a}\right)^2 + \left(\frac{n\pi}{b}\right)^2 \right\} a(z) = \frac{-\omega^2}{c^2} a(z)$$

(15)

with $a'(0) = i\omega$

$a'(-H) = 0$

Putting

$$\lambda_{mn} = \sqrt{\left(\frac{m\pi}{a}\right)^2 + \left(\frac{n\pi}{b}\right)^2 - \frac{\omega^2}{c^2}}$$

the solution for ϕ is given by

$$\phi = i\omega \frac{\cosh\left[\lambda_{mn}(z - H)\right]}{\lambda_{mn} \sinh(\lambda_{mn}H)} a_{mn}(t) \sin\frac{m\pi x}{a} \sin\frac{n\pi y}{b} \quad .$$

(16)

In order to evaluate the back pressure, P^b, we apply Bernoulli's equation at $z = 0$,

$$gw + \frac{\partial\phi}{\partial t} = \frac{-P_b}{\rho_b}$$

(17)

or

$$P_b = -\rho_b \left\{ g - \frac{\omega^2 \coth \lambda_{mn}H}{\lambda_{mn}} \right\} a_{mn}(t) \sin\frac{m\pi x}{a} \sin\frac{n\pi y}{b} \quad .$$

(18)

Evaluation of the Induced Pressure Due to the Primary Flow

For the velocity potential we can write the governing equation as

$$\frac{1}{c^2}\left(\frac{\partial}{\partial t} + U_\infty \frac{\partial}{\partial x}\right)^2 \phi = \nabla^2\phi$$

(19)

13

From momentum balance in z direction for the perturbed Eulerian flow

$$p = -\rho\left[\frac{\partial}{\partial t} + U_\infty \frac{\partial}{\partial x}\right]\phi \tag{20}$$

The boundary conditions on ϕ are

$$\frac{\partial\phi}{\partial z}\bigg|_\infty = 0 \quad, \qquad \frac{\partial\phi}{\partial z}\bigg|_{z=0} = \left(\frac{\partial}{\partial t} + U_\infty \frac{\partial}{\partial x}\right)w \quad, \tag{21}$$

using equation (20) we rewrite equations (19) and (21) as

$$\frac{1}{c^2}\left[\frac{\partial}{\partial t} + U \frac{\partial}{\partial x}\right]^2 P = \nabla^2 p \tag{22}$$

with

$$\frac{\partial P}{\partial z}\bigg|_{z=0} = -\rho a\left[\frac{\partial}{\partial t} + U \frac{\partial}{\partial x}\right]^2 w \quad, \tag{23}$$

$$\frac{\partial p}{\partial z}\bigg|_{z=\infty} \simeq 0 \quad. \tag{24}$$

Solution for P^i

Once again we use for w the form given by equations (7) and (8). Because of the nature of the boundary conditions [eqs. (23) and (24)] and the governing equation (22) itself, we can seek the solution p at the wall $z = 0$ for a mode ω_{mn} (call it p_{mn}) and using superposition obtain

$$P^i = \sum_m \sum_n P_{mn} \tag{25}$$

We shall therefore consider the expression for w as

$$w = a_{mn} e^{i\omega t} \sin\frac{m\pi x}{a} \sin\frac{n\pi y}{b} \tag{26}$$

and rewrite

$$w = \frac{a_{mn}}{4} [w_1 + w_2 + w_3 + w_4] \qquad (27)$$

and we write

$$w = \frac{a_{mn}}{4} [w_1 + w_2 + w_3 + w_4] \qquad (28)$$

where

$$w_j = e^{i(k)[x \cos \theta_j + y \sin \theta_j + c_1 t]} , \quad j = 1,2,3,4 \qquad (29)$$

and θ_j's are such that

$$\left. \begin{array}{l} \theta_1 = -\theta \\ \theta_2 = \pi - \theta \\ \theta_3 = \theta \\ \theta_4 = \pi + \theta \end{array} \right\} \qquad (30)$$

where

$$\theta = \mathrm{Min}\left[\cos^{-1}\left[\frac{m\pi}{a|k|}\right]\right] \qquad (31)$$

$$|k| = \frac{m\pi}{a} \beta_{mn} \qquad (32)$$

$$\beta_{mn} = \sqrt{1 + \left(\frac{n}{m} \frac{a}{b}\right)^2} \qquad (33)$$

and

$$c_1 = \frac{\omega}{|k|} = \frac{\omega a}{m\pi\beta_{mn}} \qquad (34)$$

In order to evaluate the induced pressure at the wall we compute the pressure due to w_i.

The solution of equation (2) with equations (23) and (24) for an input wall function w is given by

$$P(z,x,y,t) = \sum_m \sum_n \sum_{j=1}^4 a_j^{mn} \, e^{-|k| \beta_j z} \, e^{i|k|[x \cos \theta_j + y \sin \theta_j - c_1 t]} \tag{35}$$

where

$$\beta_j = \sqrt{1 - \left(\frac{U \cos \theta_j + c_1}{c}\right)^2} \tag{36}$$

$$a_j^{mn} = \frac{-\rho_a |k| [c_1 + U \cos \theta_j]^2}{\sqrt{1 - \left(\dfrac{c_1 + U \cos \theta_j}{c}\right)^2}} \; \alpha_j \, \frac{a_{mn}}{4} \tag{37}$$

with $\alpha_1 = 1$, $\alpha_2 = 1$, $\alpha_3 = -1$, and $\alpha_4 = -1$. The wall induced pressure is, therefore, given by

$$p^i = \sum_m \sum_n \sum_{j=1}^4 a_j^{mn} \, e^{i|k|[x \cos \theta_j + y \sin \theta_j + c_1 t]} \tag{38}$$

Evaluation of the Divergence Speeds for Subsonic Flows Where M << 1

We shall investigate the nature of the induced pressure p^i for subsonic flows with M << 1:

1. For $\omega = 0$ (for $m = 1$, $n = 1$) we obtain

$$p^i = a_{mn} \times \rho_a c^2 |k|^2 \frac{M^2}{\sqrt{1 - M^2}} \sin \frac{m \pi x}{a} \sin \frac{n \pi y}{b} \tag{39}$$

16

2. For nonzero ω

$$p^i = p^i_{real} + i\, p^i_{imaginary}$$

The imaginary term acts as a severe damping term.

The critical speed can therefore be defined as the speed at which the membrane goes into zero frequency flutter. Since frequency is zero, the lowest critical speed for the structure occurs when the induced pressure p^i is equal to the stiffness of the structure. Thus,

$$\frac{D\left[\left(\frac{\pi}{a}\right)^2 + \left(\frac{\pi}{b}\right)^2\right]^2 + T\left[\left(\frac{\pi}{a}\right)^2 + \left(\frac{\pi}{b}\right)^2\right]}{\rho_a c^2\left[\left(\frac{\pi}{a}\right)^2 + \left(\frac{\pi}{b}\right)^2\right]} = \frac{M^2}{\sqrt{1 - M^2}}. \tag{40}$$

For a given ratio of $\left(\frac{h}{a}\right)$ the flutter boundary (i.e., critical speed) can be found from equation (40).

Nonlinear Effects

The linear model is only capable of specifying the divergence speed. In an actual experiment one would see membrane divergence and small frequency flutter around the critical speed. This is because the nonlinear effects have not been included in developing equation (38); also, the critical speed will be slightly higher than that predicted by equation (38) since the effect of nonlinearity is to increase the stiffness. In order to obtain a valid analysis one has to:

1. Assume that a_{mn} are slowly varying functions of time, and conduct an analysis using Kelvin's stationary phase method to obtain closed form solutions; or

2. Develop numerical analytic solutions from p based on Fourier transform techniques (see ref. 15).

In many compliant experiments reported in the literature (refs. 4 and 5), the compliant model consisted of a very thin membrane (thickness $\sim$ 1 mil) bonded to a soft foam (E $\sim$ 200 psi) of thickness 0.25 to 0.5 inches. The analysis of the "laminated" structure is performed using proper structural modelling. In the following we present different approaches in modelling the structure and their basic merits.

Approximate Analytical Model

Consider (fig. 4) a membrane (a $\times$ b $\times$ h) with properties (P_m, E_m, ν_m) under uniform tension T which is bonded to a substrate (a $\times$ b $\times$ H) of properties (P_s, E_s, ν_s). We assume that the substrate can be modelled as a semi-infinite foundation undergoing plain strain deformations to external loading p(x,y,t). The end effects near the edges are thus neglected. The effective foundation properties are

$$E_f = \frac{E_s}{1 - \nu_s^2} \ , \qquad \nu_f = \frac{\nu_s}{1 - \nu_s^2} \qquad (41)$$

Of the load p(x,y,t) acting on the membrane we assume that a portion q(x,y,t) is transmitted to the foundation. The deformation state of the foundation is therefore assumed as

$$\left. \begin{array}{l} u(x,y,z,t) = v(x,y,z,t) = 0.0 \\ w(x,y,z,t) = W(x,y,t)\psi(z) \end{array} \right\} \qquad (42)$$

where W(x,y,t) is the deformation of the midplane of the membrane.

The function $\psi(z)$ is such that

$$\left. \begin{array}{l} \psi(0) = 1.0 \\ \psi(H) = 0.0 \end{array} \right\} \qquad (43)$$
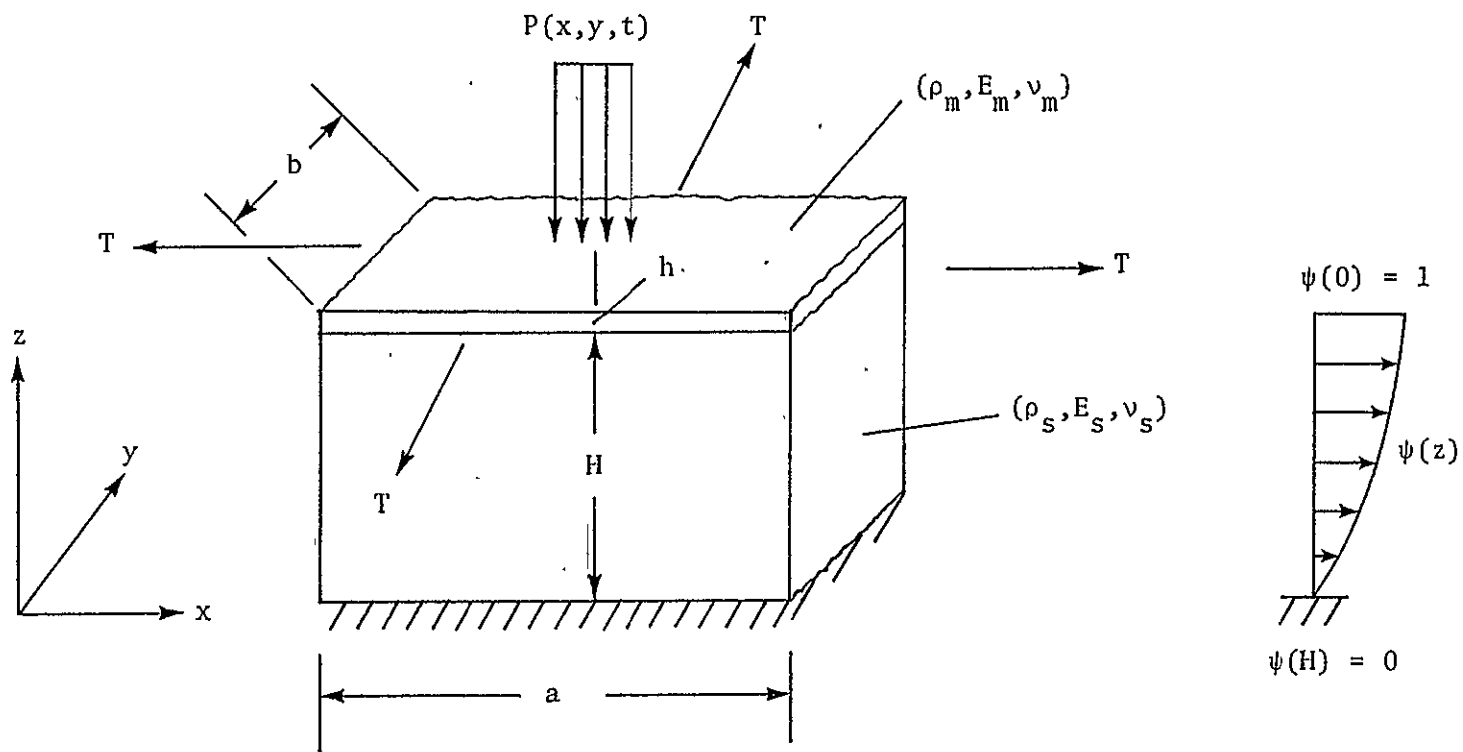
Figure 4. Laminated structure.

The functional form chosen for ψ is

$$\psi(z) = \frac{\sinh \upsilon(H - y)}{\sinh \upsilon H} \tag{44}$$

where υ is a foundation constant. The stress components of the foundation are

$$\sigma_z = \frac{E_f}{1 - \nu_f^2} \frac{\partial w}{\partial z} = \left(\frac{E_f}{1 - \nu_f^2}\right) w\psi'$$

$$\tau_{zy} = \frac{E_f}{2(1 + \nu_f)} \frac{\partial w}{\partial y} = \frac{E_f}{2(1 + \nu_f)} \psi \frac{\partial W}{\partial y} \tag{45}$$

$$\tau_{zx} = \frac{E_f}{2(1 + \nu_f)} \frac{\partial w}{\partial x} = \frac{E_f}{2(1 + \nu_f)} \psi \frac{\partial W}{\partial x}$$

Applying the principle of virtual work, the equation of motion of the substrate under the given loading $q(x,y,t)$ is obtained as

$$\int_o^H \left(\frac{\partial \tau_{zx}}{\partial x} + \frac{\partial \tau_{zy}}{\partial y}\right) \psi dz - \int_o^H \sigma_z \psi' dz - \rho_f \int_o^H \frac{\partial^2 W}{\partial t^2} \psi^2 dz = -q(x,y,t) \tag{46}$$

Equation (46) can be written as

$$q(x,y,t) = m^* \frac{\partial^2 W}{\partial t^2} + k^* W - T^* \nabla^2 W \tag{47}$$

where

$$m^* = \rho_f \int_0^H \psi^2 dz$$

$$k^* = \frac{E_f}{(1 - \nu_f^2)} \int_0^H [\psi']^2 \, dz \quad \right\} \quad (48)$$

$$T^* = \frac{E_f}{2(1 + \nu_f)} \int_0^H \psi^2 dz$$

The equation of motion of the membrane can now be developed as

$$\rho_m h \frac{\partial^2 W}{\partial t^2} + D\nabla^4 W - T\nabla^2 W = p(x,y,t) - q(x,y,t) \qquad (49)$$

where

$$D = \text{flexural rigidity} = \frac{E_m h^3}{12(1 - \nu_m^2)} \qquad (50)$$

or, using equation (48),

$$(\rho_m h + m^*) \frac{\partial^2 W}{\partial t^2} + D\nabla^4 W - (T + T^*)\nabla^2 W + k^* W = P(x,y,t) \qquad (51)$$

The eigenvalues of the structure can be determined from equation (51) as

One of the chief merits of an analysis such as the one above is its simplicity. However, the fidelity of the solution so developed depends strongly on the correct choice of the foundation parameter υ.

Models Based on Simulation Techniques

An implicit assumption in the preceding section was the one-dimensional (depthwise) variation of all deformations. The foundation thus acts basically as a series of vertical springs supporting the membrane. The finite nature of the structure makes the approximation carried out in that section rather inaccurate. A proper approach to modelling would be using a numerical technique, viz. finite elements.

Using NASTRAN (acronym for NASA Structural Analysis Program) we performed simulation studies on the laminated structure. The basic models are briefly described below.

Two-dimensional model. The structure is assumed to be two-dimensional (X-Z) in the direction of the flow (fig. 5a). The membrane is modelled as bar elements (CBAR) with only flexural properties. The substrate is assumed to develop only shear deformations due to the external loading; hence, quadrilateral membrane elements (CQDMEM) are used to model that. OFFSET cards are used to account for the offset of a node of the membrane element of the substrate from the node of the bar element at the interface.

Plate-spring model. A static three-dimensional analysis is made for an elastic slab (substrate) using three-dimensional isoparametric elements (CIHEX3) (see fig. 5b). From the static analysis the equivalent spring stiffnesses of the foundation are obtained. The membrane is modelled as a plate with membrane action (CQUAD1). For a given loading the structure (CQUAD1-CELAS) is analyzed using NASTRAN. The inertia effects of the substrate are lumped to grid points using CONM2 cards.

Fully three-dimensional model. The substrate is made up of three-dimensional isoparametric elements (NASTRAN level 15-9) CHEXA2, and the membrane is modelled by CQUAD1. The offset between the plate grid points and the surface grid point of the three-dimensional elements is neglected.
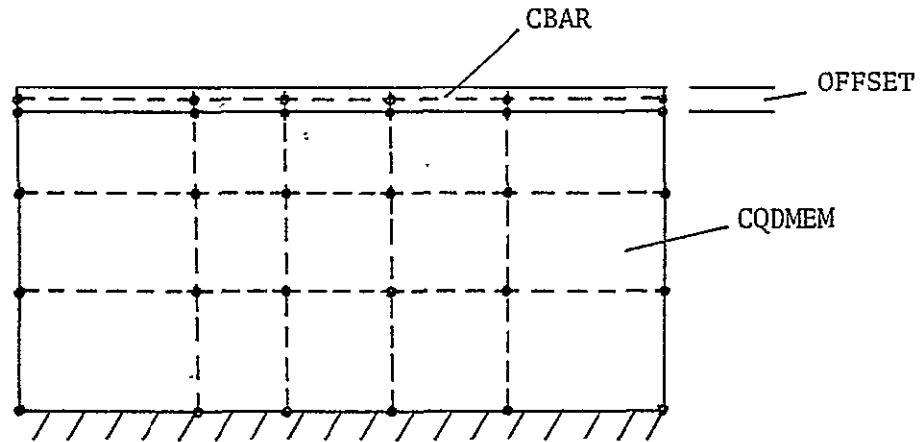
(a)
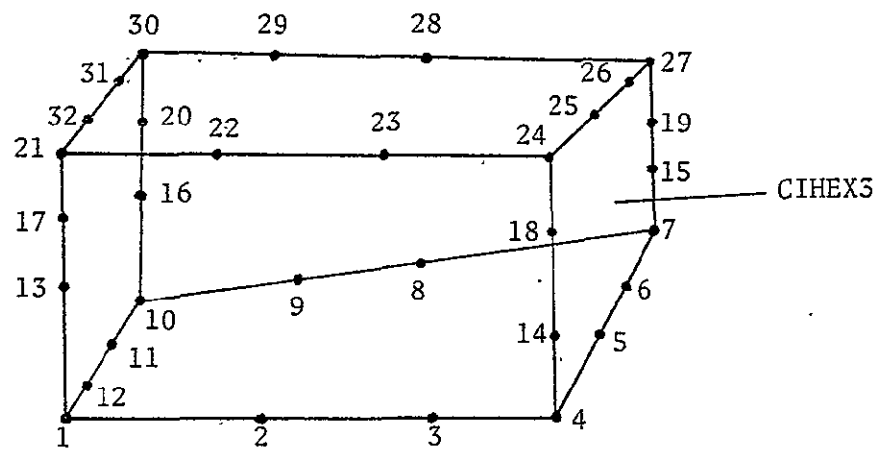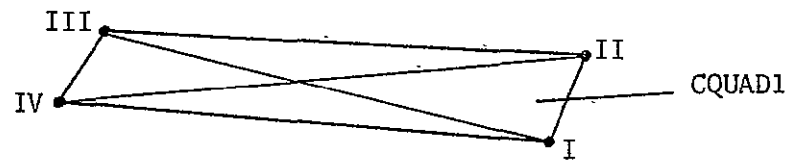
(b)

Figure 5. Quadrilateral plate element and isoparametric element with 32 grid points.

One of the major considerations in developing compliant models for tests in the new 7 × 11 wind tunnel has been the ability of the surfaces to undergo small wavelength motions. Such motions are "favorable" for drag reduction according to the criterion of the Bushnell mechanism (ref. 1). In order to facilitate small wavelength motions, a membrane under narrow a narrow air gap was tested at the Langley 7 × 11 tunnel. A drag reduction of about 10 percent was obtained in this test. The compliant model is shown in figure 6a. In figure 6b we indicate the development of small wavelengths due to chopping at the bottom. In the absence of the narrow air gap the deflected profile would have been as indicated in figure 6c.

The governing equation of motion for a membrane under a narrow air gap is

$$\rho h \frac{\partial^2 w}{\partial t^2} + D\nabla^2\nabla^2 w - T\nabla^2 w \approx P(x,y,t) \tag{53}$$

with

$$\left.\begin{aligned} w(x,y,t) &= -\delta \\[2ex] \frac{\partial w}{\partial t}(x,y,t) &= 0 \end{aligned}\right\} \quad t_1 \leq t < t_2 \tag{54}$$

where

$$\left(w(x,y,t_1) + \delta\right) \leq 0$$

and

$$t_2 \approx t_1 + \varepsilon$$

where ε is a very short duration of time whose value can be obtained through analysis of a dynamic Hertz contact problem.

The motion of the membrane under these conditions is highly nonlinear. Hence no close form solutions are possible. A finite difference solution

MEMBRANE (a × b × h, E,ρ,ν)

AIR GAP

(a)

DEFLECTED
SHAPE

(b) Development of small wavelengths

(c) Deflected profile in air (for an
unrestrained membrane)
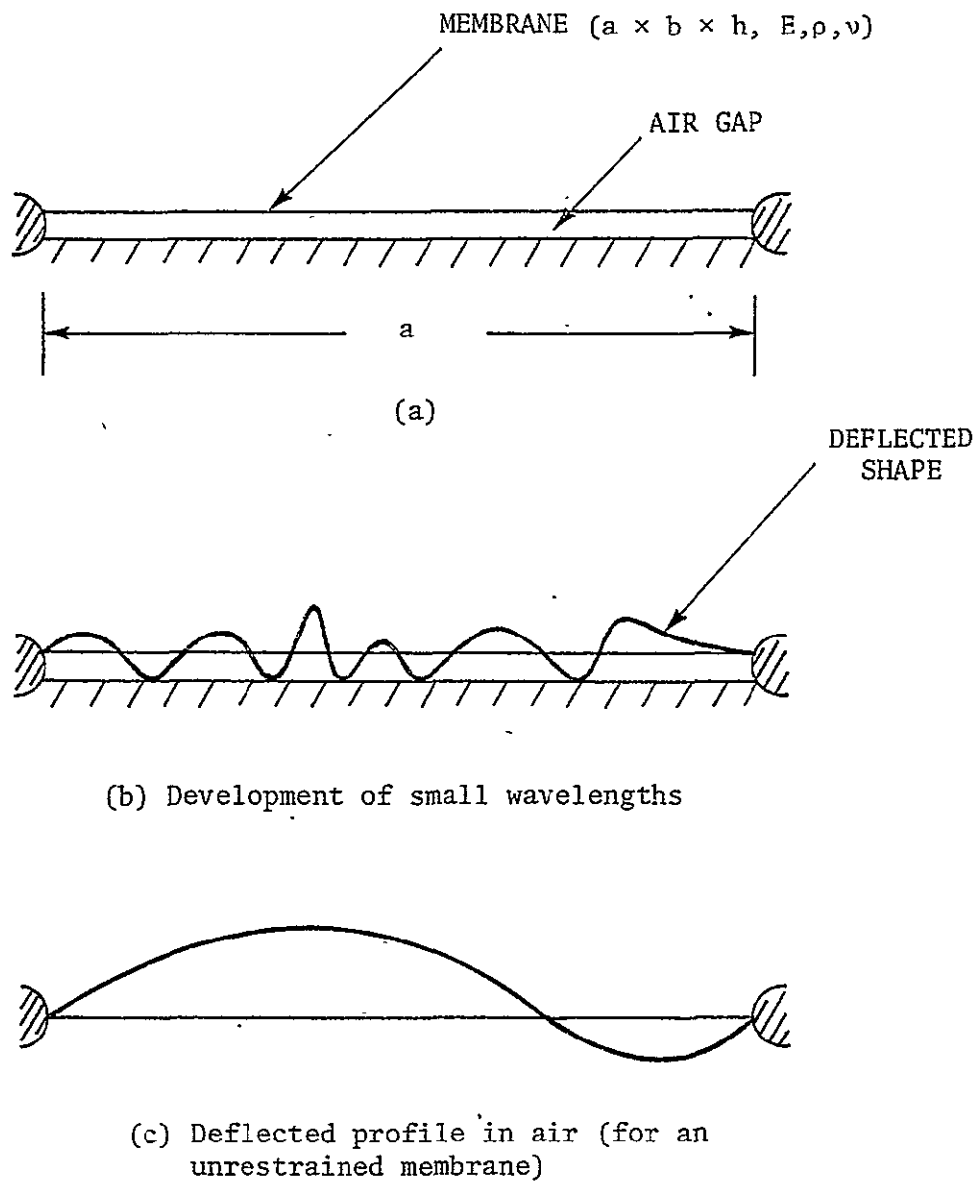
Figure 6. Membrane over narrow air gap.

for equation (53) is possible, and an algorithm with leapfrog differencing in time and center differencing in space was used to solve equation (53). The C-F-L limitation imposes

$$\frac{\Delta x}{\Delta t} \geq C_{sh} \tag{55}$$

For analysis, the bending rigidity of the membrane is neglected. An appropriate choice for Δt has been made as

$$\left. \begin{array}{l} \Delta t = \dfrac{\Delta x}{5 C_{sh}} \\[2em] \text{where} \\[2em] C_{sh} = \sqrt{\dfrac{T}{\rho h}} \end{array} \right\} \tag{56}$$

For analysis Δx was chosen equal to Δy (uniform mesh spacing), and the value of Δx was chosen to obtain resolution of the smallest wavelength possible. The numerical model consisted of a 10 in. × 10 in. membrane with an air gap thickness, $\delta = 10^{-4}$ in. The smallest wavelength we wanted to capture was of length $\lambda = 2$ in. Thus, the mesh spacing was set at $\Delta x = 0.2$ in.

A one-dimensional analysis of the same problem is possible with greater resolution of wavelengths. Here one would assume variations in the y direction to be unimportant. However, the one-dimensional analysis can only show trends, since the nonlinear nature of the problem prohibits comparisons between the one-dimensional analogue of equations (53) and (54), and the two-dimensional problem.

The conclusions to be drawn from extensive simulation studies conducted are that (1) the model equations (53) and (54) have unique solutions (convergence with reduction of step size) and (2) the solution for dynamic response exhibits small wavelength, high frequency motions compared to a pure membrane.

Compliant drag reduction has been reported in the literature for periodically supported structures (ref. 2). The length of the bays for these compliant surfaces corresponds to the wavelengths predicted by the Bushnell mechanism. We develop below an analytic method of solution for periodic structures based on the work of Mead and Pujara (ref. 15).

The theory developed here is basically a linear small deflection theory with the requirement from consideration that the midplane strains are negligible, i.e., $\frac{w}{h} \ll 1$. We will therefore discard solutions which give amplitudes $w \sim O(h)$ or greater. The above requirement is essential, as the ratio of the linear restoring force versus the nonlinear stretching force needs to be very large, i.e.,

$$w \times \frac{Eh^3}{12(1 - v^2)} \left(\frac{2\pi}{\lambda}\right)^4 \gg w^3 \, Eh\left(\frac{2\pi}{\lambda}\right)^4$$

or (57)

$$\frac{w^2}{h^2} \ll 1 \quad .$$

We also assume a priori that the structure is one-dimensional, i.e., crossflow directional variations are neglected ($a/b \ll 1$).

Figure 7a shows a periodically supported beam, over which is a flow with speed U_∞. Figure 7b shows an equivalent representation for flexibility at the supports and sitting on an elastic foundation (stiffnes = k_f). If the foundation is viscoelastic the representation for the foundation is made $k_f' = k_f(1 + i \, n_f)$ where n_f is a typical "loss factor" for the foundation and k_f' is the complex stiffness of the foundation.

We shall develop the theory of response of the structure for two cases:

1. The foundation is absent; instead there is a cavity of fluid at the backing, and

2. The case with the foundation.

$(\ell_x h,\ E,\nu,\rho)$
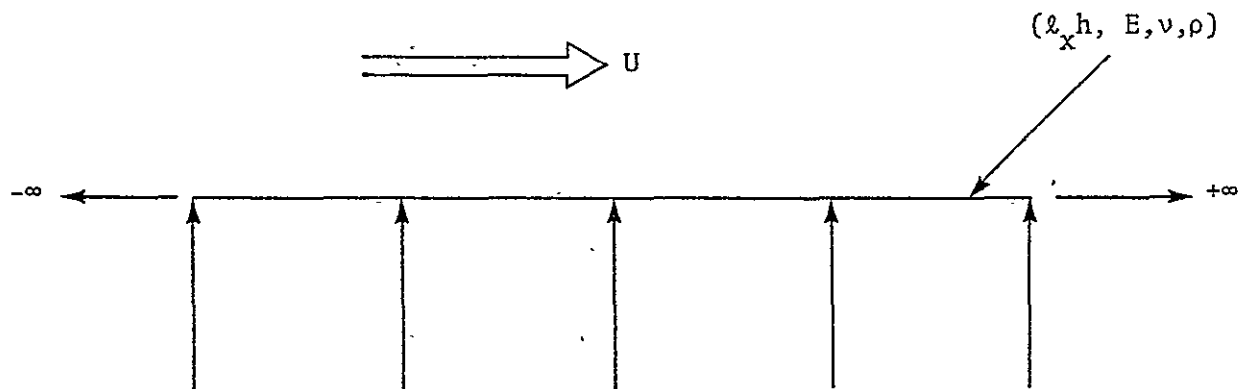
(a) Periodically supported beam
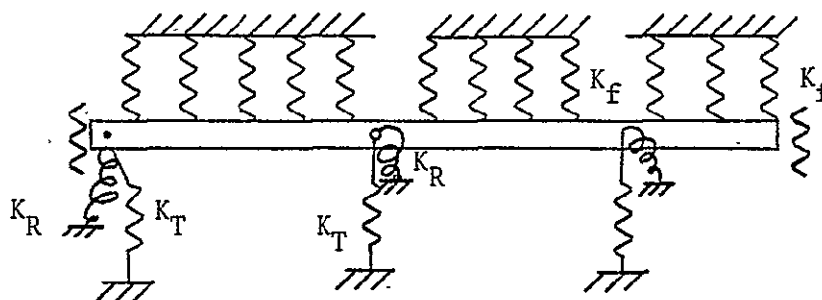
(b)

Figure 7. Equivalent representation for a beam on elastic foundation.

Case 1. To develop expressions for this case one has to evaluate the reaction of the cavity P_b on the bay under consideration. The approach is very similar to evaluation of the induced pressure p^i acting on the side where there is flow and hence will not be dwelled upon in detail here. Also, one has to set the foundation reaction (k_f = 0) to zero.

Case 2. Consider an external force field

$$p^e = P_o e^{-i\mu \frac{x}{\ell}} e^{i\omega t} \tag{58}$$

We seek harmonic solutions to the excitation. The transverse displacement can be written as

$$w(x) = \sum_{n=-\infty}^{\infty} A_n e^{-i(\mu+2n\pi)\frac{x}{\ell}} e^{i\omega t} \tag{59}$$

We shall assume that the flexural rigidity of the beam is D'

$$D' = D(1 + i n_b) \tag{60}$$

where η is the loss factor for the beam and $D = \dfrac{Eh^3}{12(1 - \nu^2)}$. The equation of motion of the beam under consideration of excitation is

$$D' \frac{\partial^4 w}{\partial x^4} + \rho_b h \frac{\partial^2 w}{\partial t^2} + k_f' w = P^e(x,t) + P^i(x,t) + R_1 \delta(x) + R_2 \delta(x - \ell) \tag{61}$$

where R_1 and R_2 are the reactions of the supports and P^i is the induced pressure. The induced pressure can be evaluated as was done in previous sections as

$$p^i(x,t) = \sum_{n=-\infty}^{\infty} \frac{\rho_1 \omega^2}{i \overline{k}_n} A_n e^{i[\omega t - \mu n(\frac{x}{\ell})]} \tag{62}$$

where ρ_1 is the density of the fluid medium,

$$\overline{k}_n = \sqrt{\left(\frac{\omega}{\ell}\right)^2 - \left(\frac{\mu_n}{\ell}\right)^2}$$

(63)

and 'a' equals the speed of sound in the medium,

$$\mu_n = \mu_o + 2n\pi$$

(64)

In order to obtain solution of equation (61) for given loading [equation (58)], we evaluate the virtual work done by virtual displacement $\delta A_m\, e^{i(\mu m \frac{x}{\ell} - \omega t)}$ and equate the sum of all virtual work to zero. Because of the periodicity of the bays the total virtual work done by the supports to be included in a single bay is just due to that of one of the supports.

The virtual work done by the support at x = 0 is

$$\delta\omega_R = \delta A m \left\{ K_t' \sum_{n=-\infty}^{\infty} A_n + K_r \sum_{-\infty}^{\infty} A_n \frac{\mu_m \mu_n}{\ell^2} \right\}$$

(65)

The virtual work done by the other reactive forces can be obtained by multiplying equation (61) by the virtual displacement and integrating over the interval 0 to ℓ. Finally, we indicate the set of simultaneous equations obtained by setting the sum of all virtual work to zero as

$$A_m \left[D' \left(\frac{\mu_m}{\ell}\right)^4 - \rho_b h + \left(\frac{\rho_1}{ik_m}\right) \omega^2 \right] + \frac{K_t'}{\ell} \sum_{n=-\infty}^{\infty} A_n$$

$$+ \frac{k_r}{\ell^3} \left[\sum_{-\infty}^{\infty} A_n \frac{\mu_m \mu_n}{\ell^2} \right] = 0 \quad \text{when } m \neq 0$$

(66)

$$= p_o \quad \text{when } m = 0$$

The simultaneous set of equation (66) can be solved finally to obtain A_i. In practice, only a few of these A_i's have to be evaluated. Taking n to be between -6 to +6 is sufficient to obtain the desired accuracy. Usually the rotational rigidity of the supports is zero (simply supported, i.e., $Kr = 0$) we indicate here the approach which is simple to solve equation (66) for this case.

We rewrite equation (66) as

$$\left. \begin{array}{ll} A_m \phi_m + \frac{K'}{\ell} \sum A_n = P_o & m \neq 0 \\[3mm] \qquad\qquad\qquad = 0 & m = 0 \end{array} \right\} \tag{67}$$

where

$$\phi_m = \left(\frac{\mu_m}{\ell}\right)^4 D' - \Omega^2 \left(m_b + \frac{\rho_1}{i\overline{k}_m}\right) \tag{68}$$

From the case $m = 0$ we obtain

$$\sum A_n = \frac{P_o/\phi_o}{1 + \frac{K'}{\ell} \Sigma \frac{1}{\phi_n}} = K \tag{69}$$

Then

$$A_m = \frac{-k'K}{\ell \phi_m} \; ; \qquad A_o = \frac{P_o}{\phi_o} - \frac{K'k}{\phi_o} \tag{69}$$

for the case where $K_T \rightarrow \infty$ equation (69) yields in the limit

$$A_m = \frac{-P_o}{\left\{\phi_m \phi_o \sum_{-\infty}^{\infty} \frac{1}{\phi_n}\right\}} \tag{70}$$

The evaluation of A_i leads to the knowledge of $w(x)$ for a given harmonic excitation.

In order to obtain the solution for a wide band excitation one must carry out a Fourier analysis of the exciting field and sum up, using the principle of superposition, the harmonic responses given by equation (59). The wide band response can then be analyzed to obtain power spectral data of expected response. The mean square response is defined as

$$E[\omega\omega^*] = E\left\{P(\omega)P^*(\omega)\right\} \; H(j\omega)H^*(j\omega) \tag{71}$$

where $H(j\omega)$ is the frequency response function and $E\left\{P(\omega)P^*(\omega)\right\}$ is the power spectrum of the turbulent pressure field.

NUMERICAL RESULTS

In the preceding sections we have developed appropriate techniques for analysis of a generic of compliant structures. Using these analyses we examine in this section the nature of structural response under reported experimental conditions.

Laminated Structures

The compliant model tested in the LTPT tunnel at Langley consisted of an 51 in. × 18 in. model surface. The compliant surface was made of 1 mil mylar (Young's modulus $\sim 5 \times 10^5$ psi, $\nu = 0.3$) with a backing substrate which is a soft foam (80 PPI Polyurethane foam, $E \simeq 200$ psi) of thickness 0.25 in. In table 1 we report the eigenvalues (natural frequency of vibration) obtained using different models discussed in the Structural Analysis for Laminated Structures section. These eigenvalues are arranged in ascending order. Those eigenvalues listed in the last column under "Membrane" represent the natural frequency of the membrane (in vacuo) if the substrate were absent. Figure 8 presents the frequency response of the laminated structure and indicates that the amplitudes are small; the turbulent pressure excites the structure into a wide band response with most of the power included in the frequency range below its lowest natural frequency.

Table 1. Natural frequencies of a laminated structure.*

Eigenvalues	Using NASTRAN Models	Using Eq. (52)	Membrane In Vacuo
(1,1)	484.6 Hz	535.2	125.6
(2,1)	485.0	536.0	145.0
(3,1)	485.7	537.6	172.5
(4,1)	486.6	539.5	204.9
(5,1)	486.6	541.8	240.2
(1,2)	487.7	541.8	240.5
(2,2)	488.9	542.6	251.2
(3,2)	490.4	543.9	268.0
(4,2)	490.5	544.6	277.4
(6,1)	492.0	544.9	290.0

*   The membrane is 1 mil mylar, substrate 0.25 in. thick, 80 PPI PU foam
($E = 2.2$ psi, $\nu = 0.1$). The model is 51 in. × 18 in. and with a tension
on the membrane of 2 lbs/in.

** The foundation parameter υ is chosen to be 2.0
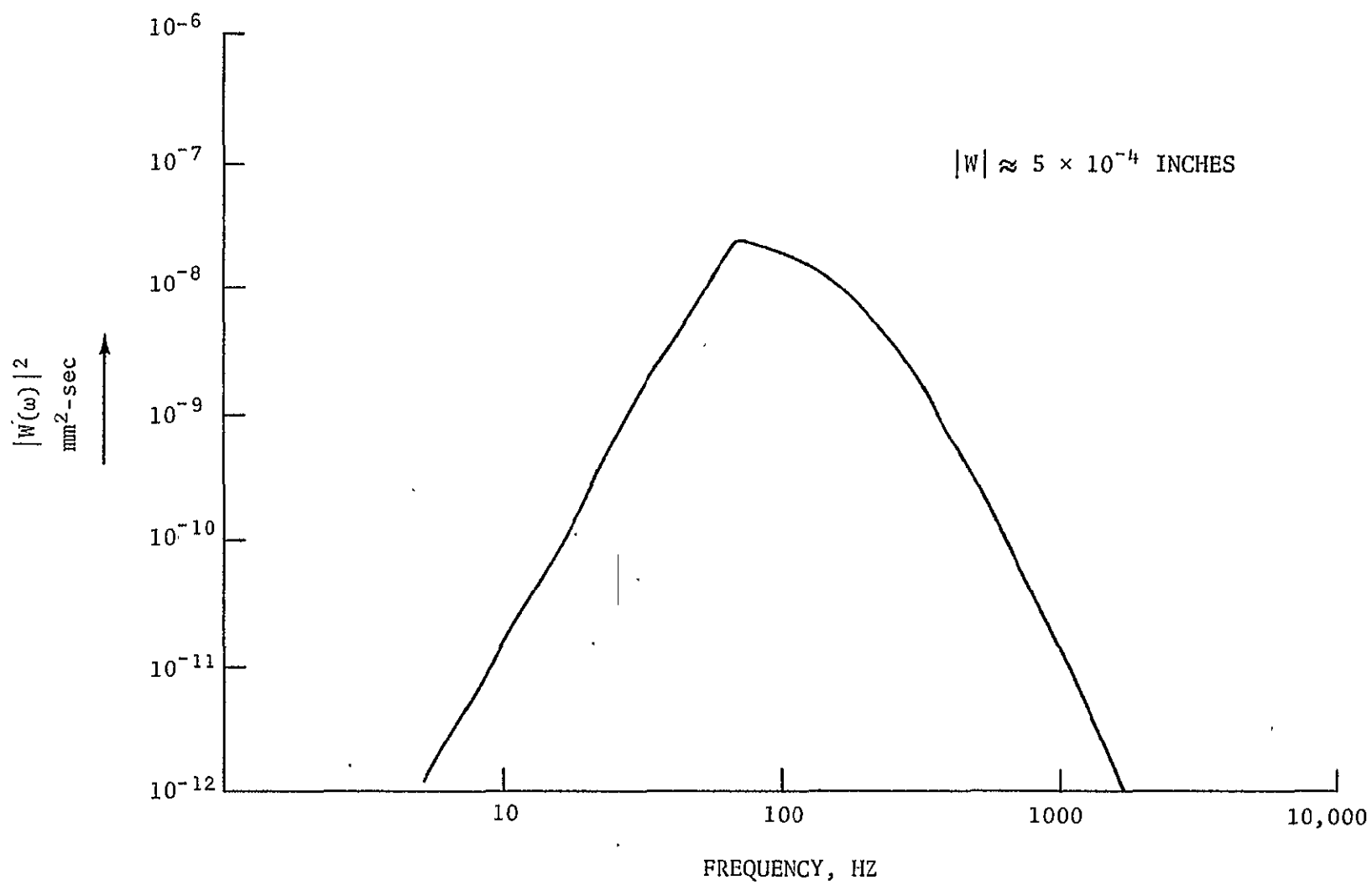
Figure 8. Frequency response of a laminated structure.

We conclude that laminated structures do not show any promise as "passive" compliant surfaces on the basis of the Bushnell mechanism.

Membranes Under Narrow Air Gap

As was indicated in the Membranes Under Narrow Air Gaps section above, the analysis of the membrane over a narrow air gap only presents qualitative information regarding the nature of the motion. Using the simulation program for pressure (ref. 14) we have developed solutions for a 10 in. × 10 in. compliant model with 1 mil (1000 μin.) mylar over 100 μin. air gap and a flow of 50 ft/sec. Such flow conditions typically occur in a 7 in. × 11 in. tunnel at Langley. The boundary layer thickness was approximately 0.5 in. The pressure history and displacement for the midpoint of the surface is indicated in figure 9 for a duration of time.

Figure 10 indicates the influence of spatial discretization on the solution obtained. Figure 11 presents an analysis of the frequency response of the motion, It is shown that the narrow air gap-membrane configuration yields high frequency motion.

Membranes Under Large Cavities

In some reported experiments (ref. 3) membranes over fluid-filled cavities have shown drag reduction. In order to understand the nature of the surface motion we examined a recent compliant wall experiment: the membrane is 1 mil thick mylar and the cavity is 0.25 in. deep and filled with air. The test speed is 50 ft/sec. The mean square response with frequency is indicated in figure 12. It is shown that the motion is purely low frequency, large wavelength. Therefore, we do not believe that membranes over large air gaps are promising candidates for compliant experiments.

Figure 13 indicates the response of a membrane with a water-filled cavity. Again the presence of the cavity shifts the response curve towards the low frequency end of the spectrum.
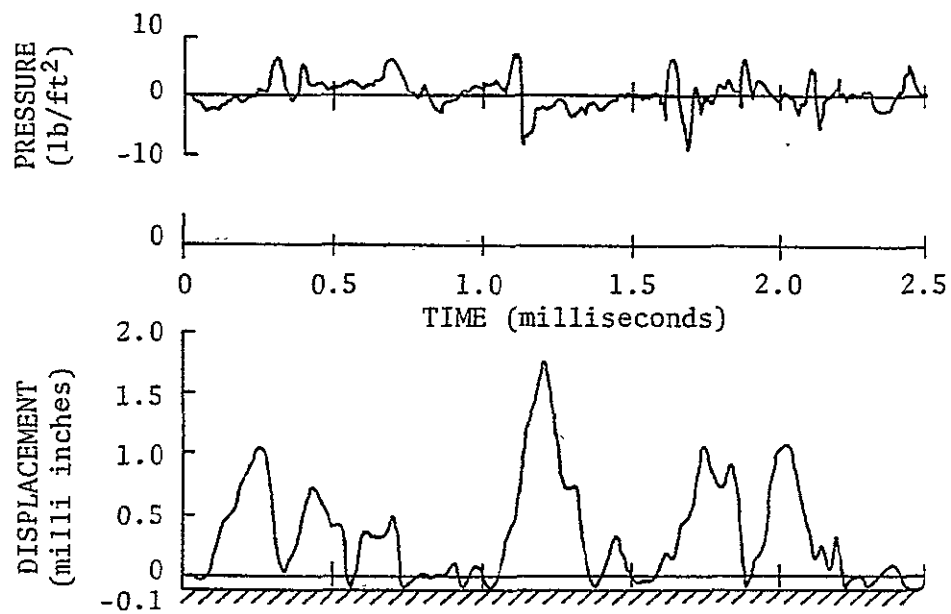
Figure 9. . The pressure history and resulting surface motion
for a membrane over an air gap (U_∞ = 15.2 m/sec,
2.54 cm boundary layer thickness).
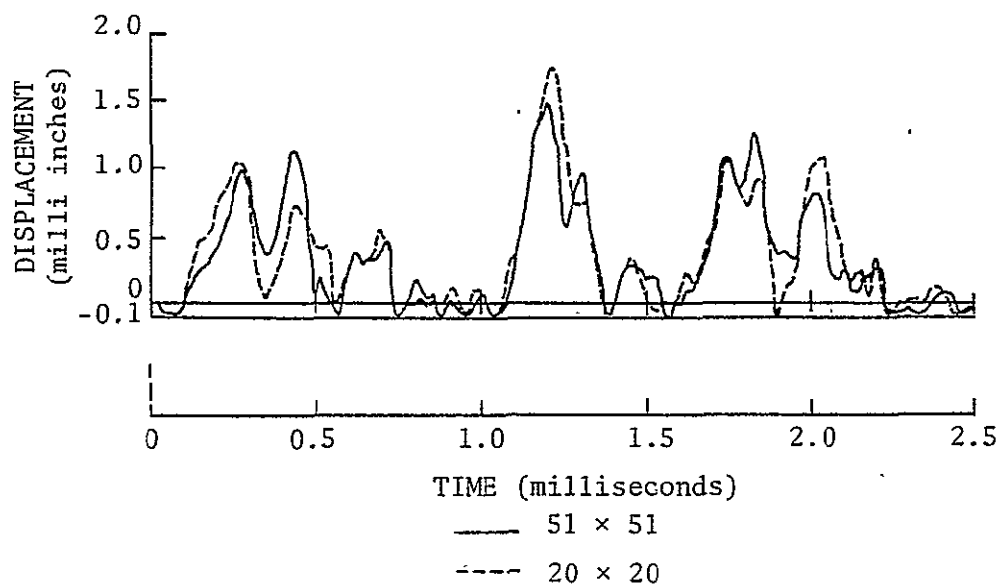
Figure 10. Influence of resolution on predicted surface motion.
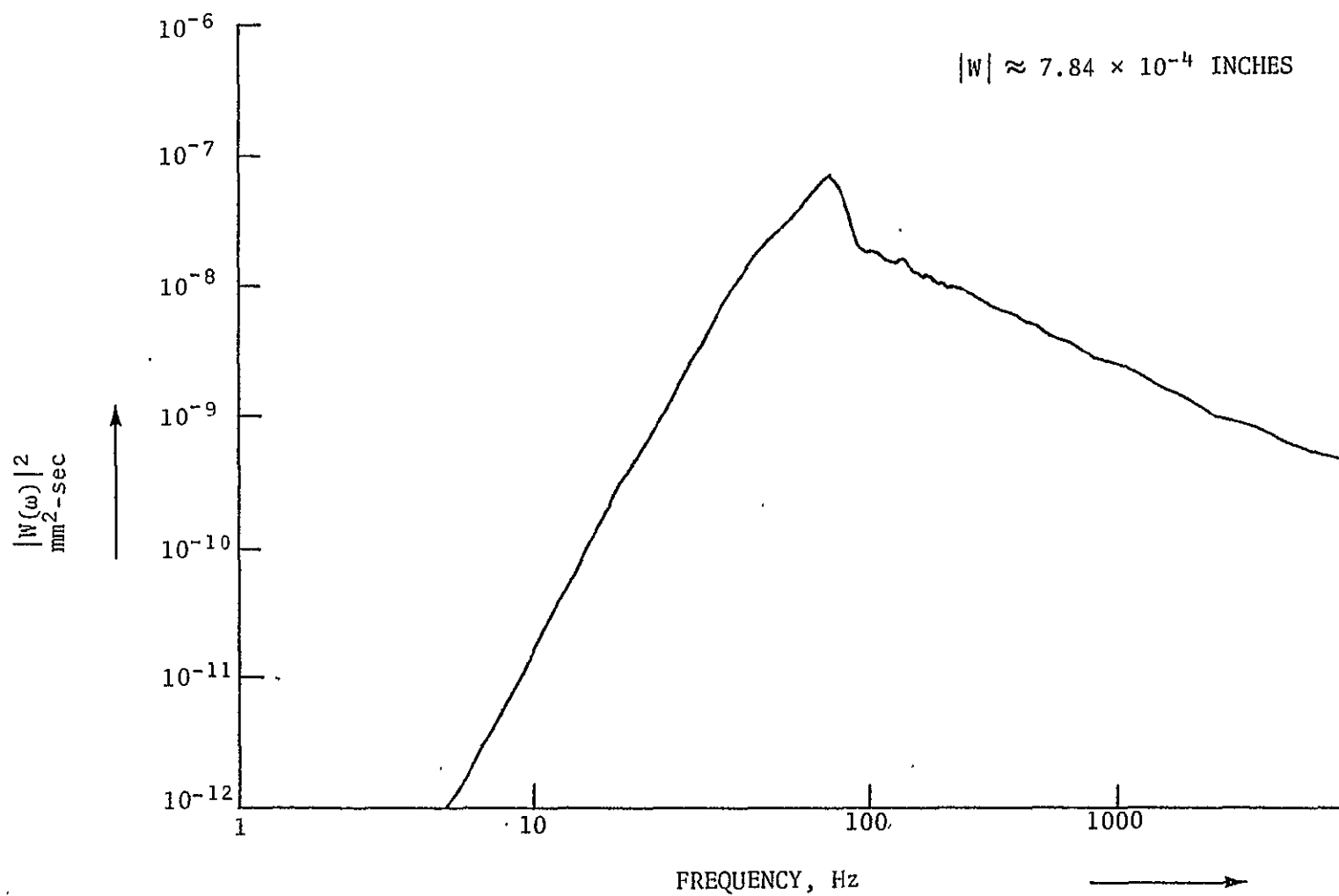
Figure 11. Membrane over narrow air gap--frequency response curve.
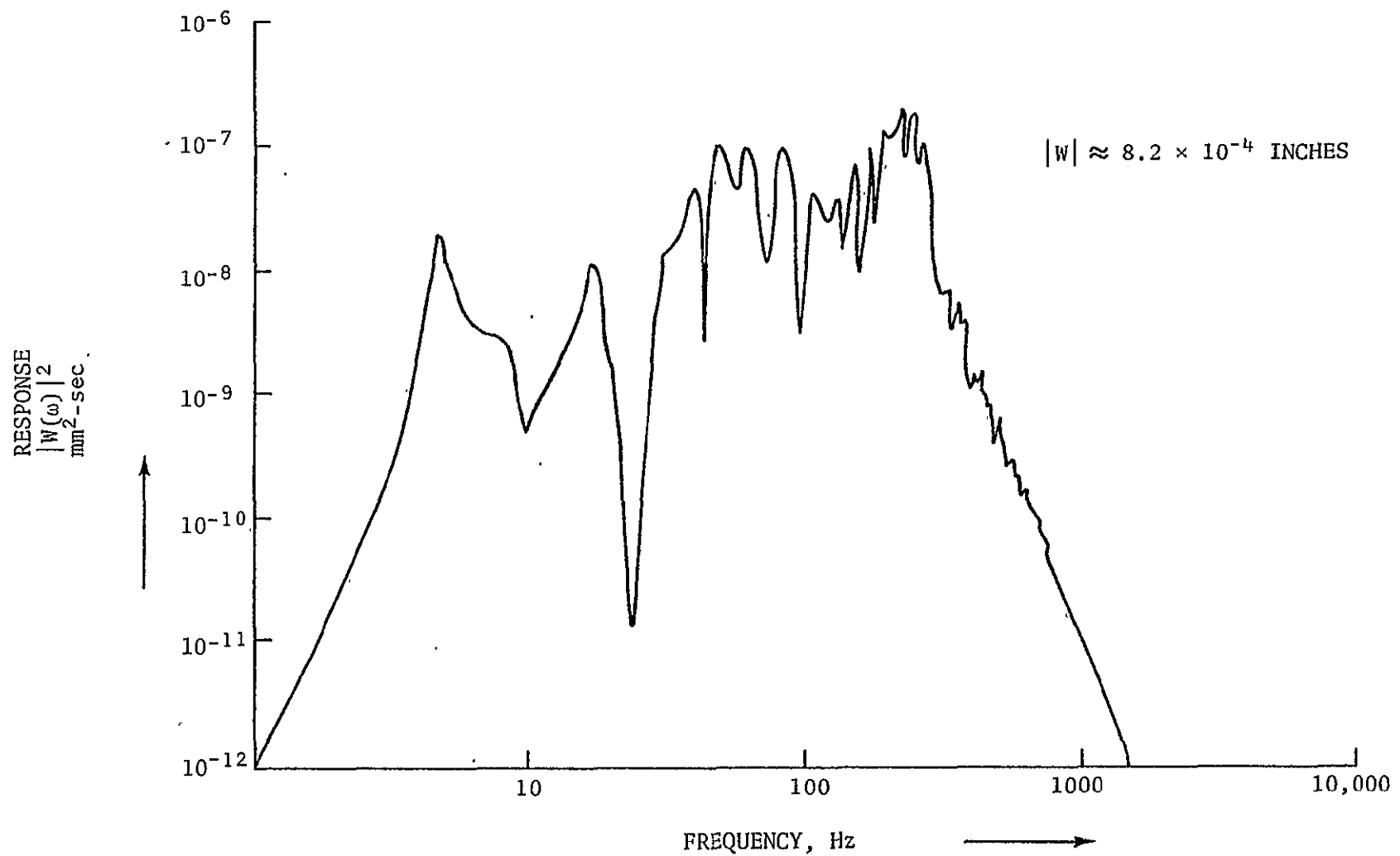
Figure 12. Membrane over large air gap--frequency response curve.

The y-axis is labeled, from bottom to top: RESPONSE AMPLITUDE $|W(\omega)|^2$ mm^2-sec

The y-axis scale values are: 10^{-14}, 10^{-13}, 10^{-12}, 10^{-11}, 10^{-10}

The x-axis is labeled: FREQUENCY, Hz

The x-axis scale values are: 1, 10, 100, 1000

$$\frac{2\pi f\delta}{U_\infty} = 1$$
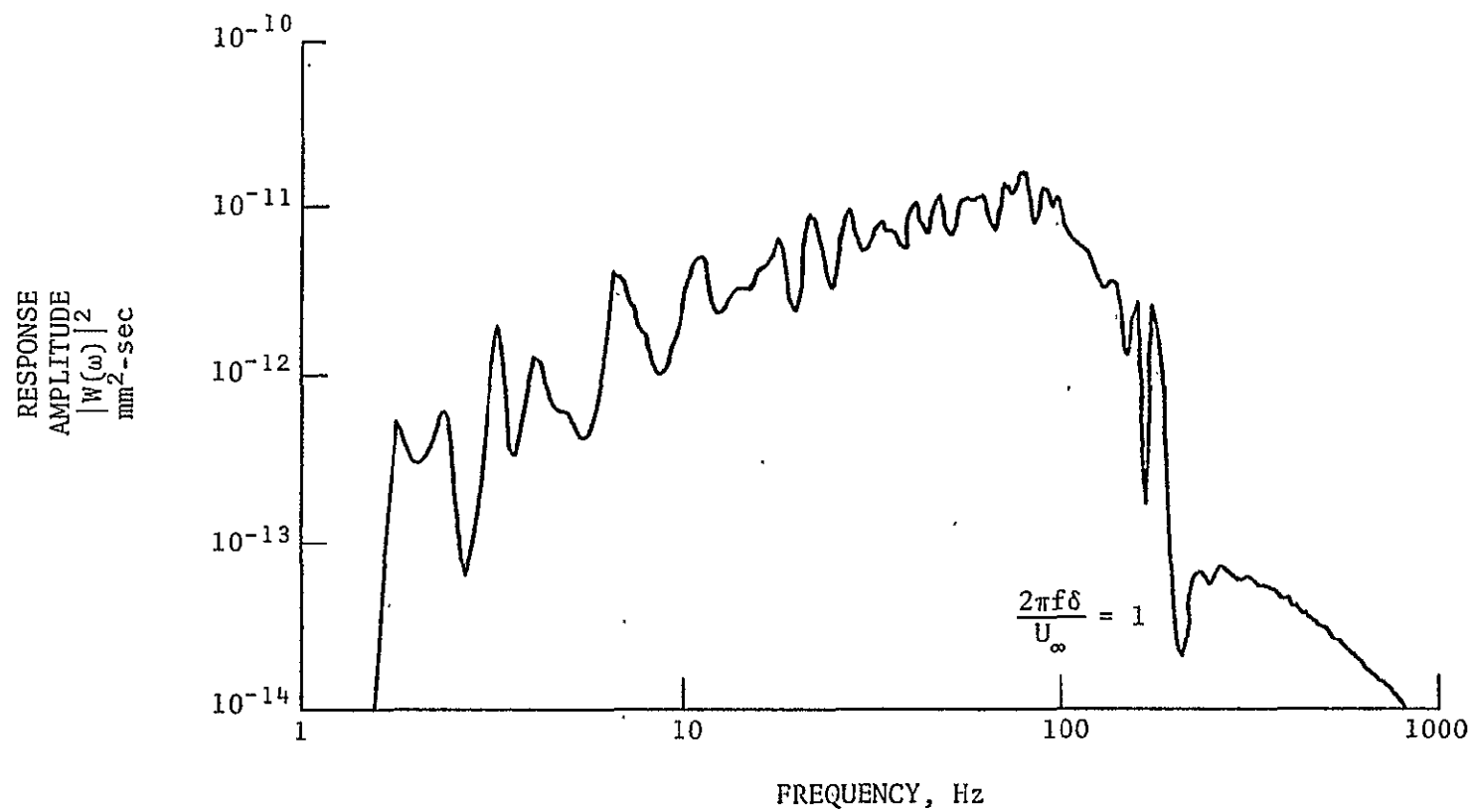
Figure 13.   Water backed membrane response.

Periodic Structures

The original reporting of compliant drag reduction (ref. 2) was for a periodic structure made of a rubber diaphragm (80 mil thick) supported on periodic stubs of rubber with water filling between the stubs. The height of the stubs was 40 mil and the width 20 mil. Using the above data we examined the surface response to turbulent flow (medium is water) at a speed of 50 ft/sec corresponding to the experiment of Kramer. Figure 14 indicates the surface response. We determined that the periodic Kramer surface was a high frequency passive surface and could have been a drag-reducing surface satisfying the conditions of Bushnell criterion. In nondimensional units our analysis indicates for the Kramer surface a λ^+ = 800, h^+ = 100, and c = 0.7 U_∞. The analysis includes a nominal value of damping for the structure. We expect, however, that the actual damping in the structure may limit the amplitude to $h^+ \sim$ 20 or 30 in the experiment. Such an excitation is capable of reducing the rate of burst production and hence could have been responsible for the observed drag reduction.

Most attempts toward reproducing the results of Kramer over the years have been unsuccessful. One of the chief reasons for this has been the belief that Kramer's experiment delays transition; hence, subsequent experiments at various laboratories were conducted as transition experiments. In a few cases the flow had been accidentally tripped to turbulence, and there have been reports that drag reduction was indeed observed for these cases. However, the majority of data points showed no favorable drag changes (ref. 17). We also emphasize that proper attention was not given to the structural motions required. Consequently, the geometries tested were not facsimiles or scale models of the Kramer surface. There is, therefore, a need for re-examining Kramer's surface for possible drag reduction.

PASSIVE WALLS FOR 7 IN. × 11 IN. TUNNEL

The 7 in. × 11 in. tunnel at Langley has a speed range of 50 to 150 ft/sec. The flow is tripped about 1 ft from the test model using rougheners (sandpaper). Boundary layer surveys on the test model indicate that a relatively thick boundary layer (δ = 0.5 to 1.0 in.) is formed on the model.

$|W| \approx 7$ mil around 1000 Hz

$$\frac{2\pi f\delta}{U_\infty} = 1$$

RESPONSE AMPLITUDE $|W(\omega)|^2$ mm^2-sec
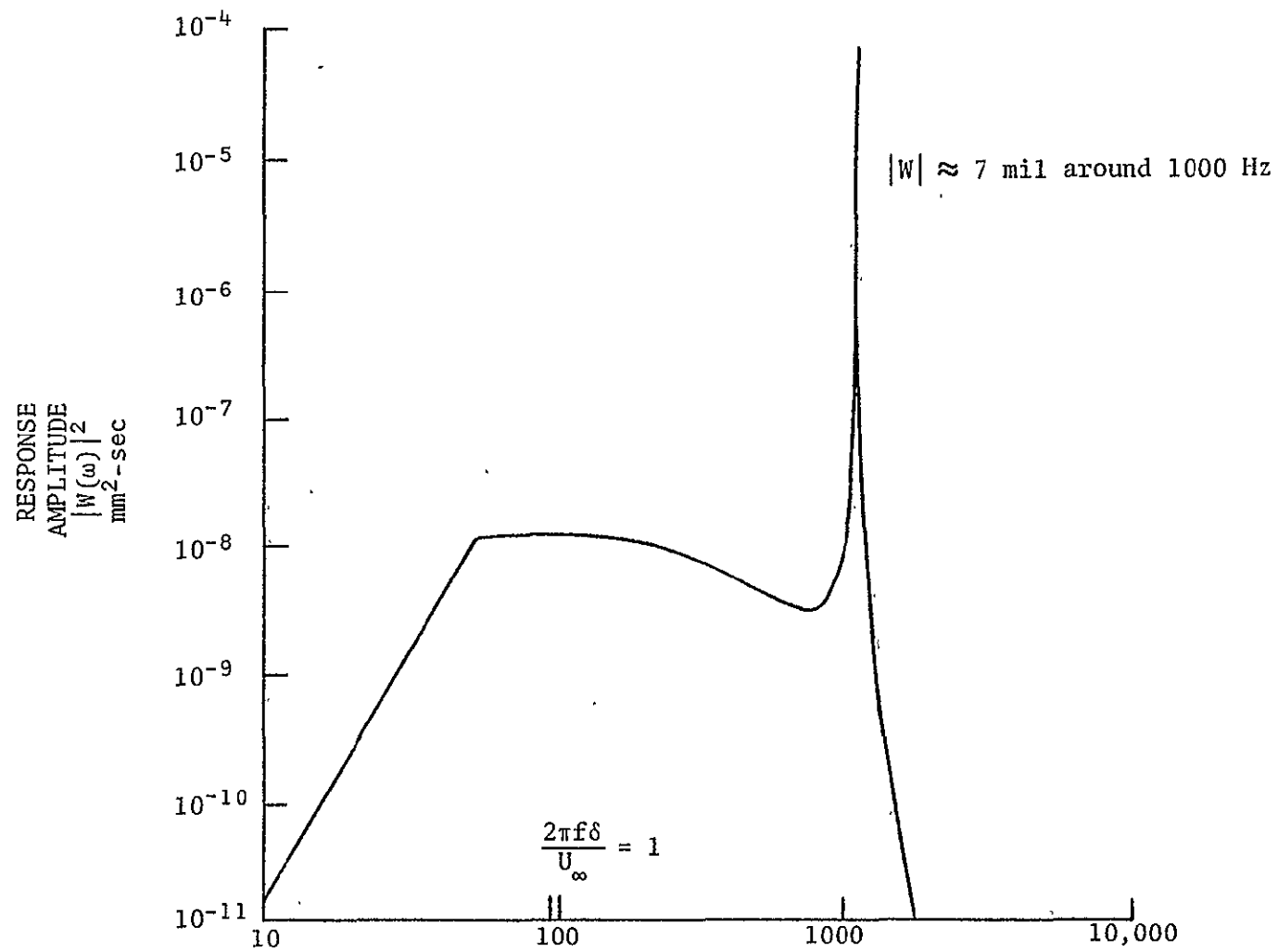
Figure 14. Steady-state response of Kramer stubbed periodic surface $(U_\infty = 18$ m/sec water flow).

The model itself is 11 in. × 36 in. and floats on a drag balance (see fig. 15).
The facing plates smoothly fan the flow onto the test area. When rigid plate
measurements are made the whole surface area is available. However, the
compliant section on which measurements are made spans only a 7 in. × 16 in.
area in order to avoid nonuniformities of flow around the side walls. The
adjustable backplate provides a facility for adjusting the cavity depth which
can be filled by a foam or with any fluid. When a backing such as air is
used, the back pressure is controlled using a vacuum pump. The overall
pressure gradient in the test region is kept at a minimum. However, there
is a slight pressure gradient of a few μ psi/in. in the tunnel test section.
The total pressure on the flow side fluctuates slightly from the ambient,
and the tunnel static pressure differs from the ambient pressure as a small
function of the flow speed under conditions of optimal operation. While
evaluating the response of structures under flow we included this small
static pressure differential acting on the structure in addition to the
existing force fields.

The vacuum section chamber in the model (fig. 15) is used to put tension
on the compliant wall. The widths of the cavity of the suction chamber are
adjusted in such a way that the tension is uniform. This gives the ratio
of the cavity widths in x and y directions as

$$\left(\frac{\ell_x}{\ell_y}\right) = \left(\frac{a}{b}\right)^{1/3} \tag{72}$$

(see Appendix B) in order to obtain uniform tension of the membrane. By
directly observing the center deflection of the membrane in the cavity on
any side and noticing the pressure differential, one can directly evaluate
the tension in the membrane knowing the properties of the membrane.

Finally, direct calibration can be made between the tension in the mem-
brane and the vacuum pressure provided that the properties of the compliant
membrane are fully known.

In figure 16 we show the observed surface motion using a schlieren system
for taking area photographs. The surface is a membrane over a narrow air
gap. The dark spots in the picture correspond to points where the membrane

BACKING PLATE

SMOOTH
FACING

36 IN.

COMPLIANT
SURFACE

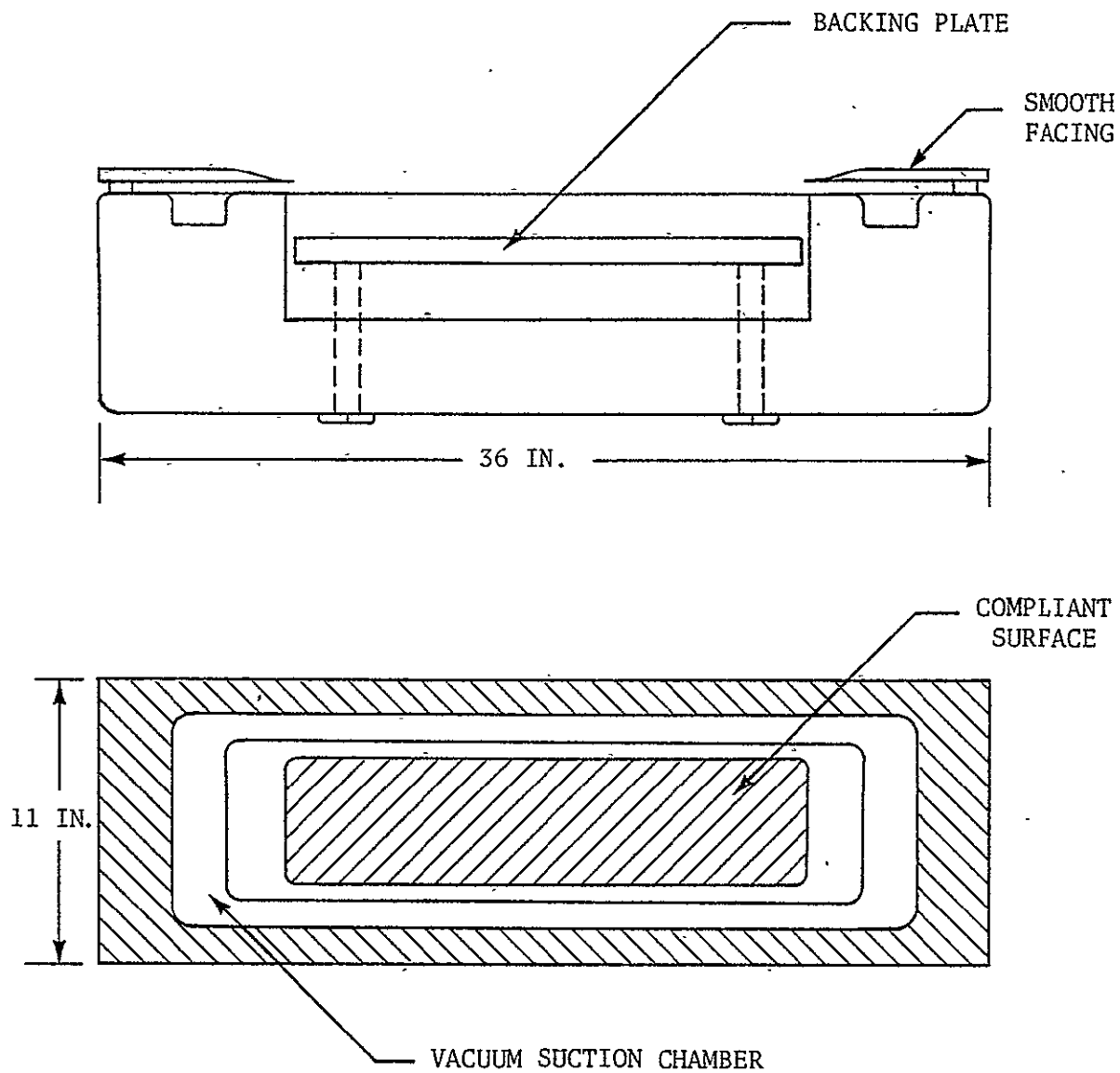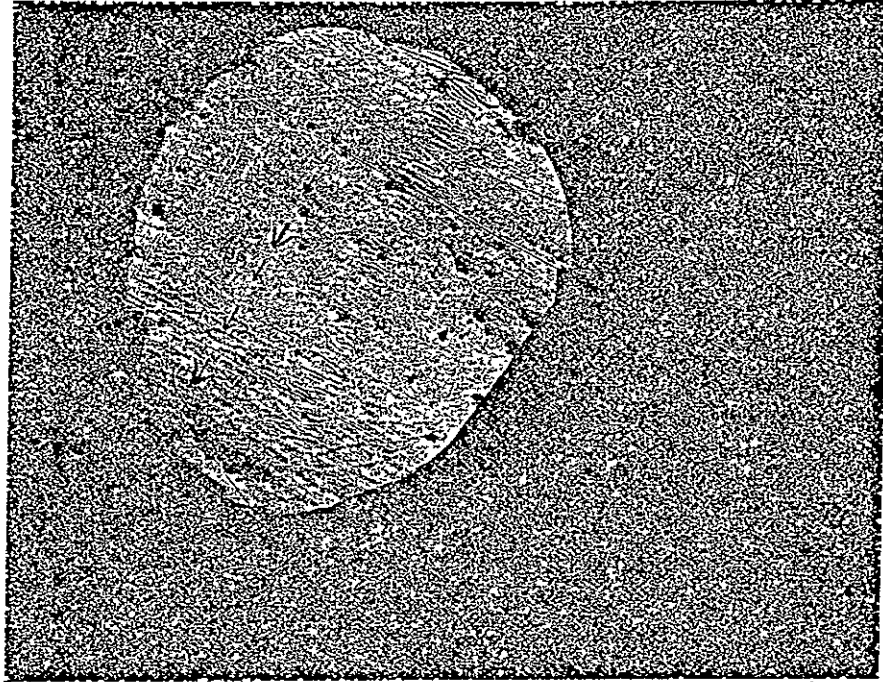11 IN.

VACUUM SUCTION CHAMBER

Figure 15.   The compliant wall model.

Figure 16. Area photograph of the response of a membrane
over a narrow air gap; backing surface is
10 PPI foam.

44

touches the 10 PPI foam surface after the excursion through the narrow air gap. The arrows indicate the direction of flow. The tension in the membrane is low.

In figure 17 we show the surface motion as a function of time at a point on the surface as seen in the oscilloscope. Each division in the screen corresponds to 5 milliseconds (in the x direction) and in the ordinate 1 division corresponds to 0.1 volts of photodetector output for the bottom picture and 0.01 volts for the top one. The output of the photodetector is directly proportional to the maximum angles of the surface motion and has been calibrated already.

From figure 17 we learn that the surface motion of the membrane over the narrow air gap is high frequency (between 400 Hz and 2 KHz) and has amplitudes of 100 μin. or more.

In figure 18 we show the area photograph of a "dulcimer" model. The model consists of a membrane sitting on periodically supporting strings. There is a separation between the membrane and the strings, and during surface oscillation the membrane slaps on the strings. The dark lines correspond to the strings in contact with the membrane. The strings are kept in tension. The motion of this surface is again small wavelength and at moderate frequencies. Figure 19 shows the motion of a point with respect to time. The time scale is 20 milliseconds/division. The flow speed is U_∞ = 160 ft/sec. Again, the surface amplitudes are only about 200 μins. (1 volt $\approx$ 100μ in.).

Using the theoretical analyses in the preceding section, we also conducted some experiments where the wall was made to flutter. (The spacings between supports were designed to be such that low frequency flutter occurred.) One of the chief problems in these experiments was adjusting the pressure in the back chamber continually while the experiment was going on, in order to suppress the panel divergence.

The models were tested for drag reduction too. In most of these compliant experiments there was little drag change. The observed motions did not suggest that the surface motion was in the range of parameters suggested by the Bushnell mechanism either. Further compliant experiments where compliant motions suggested by the Bushnell mechanism can be produced (active walls/passive walls) are underway.
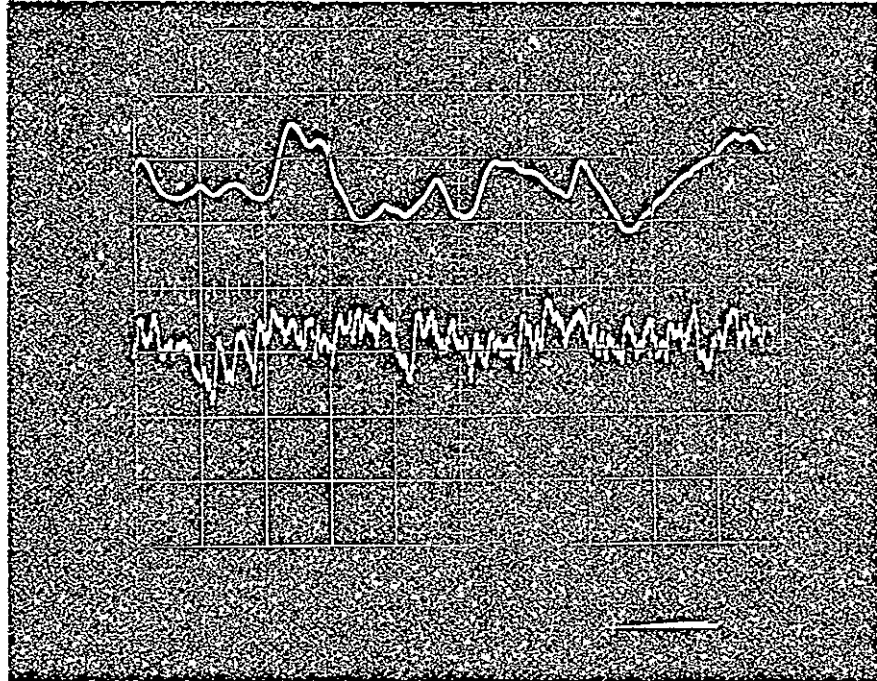
Figure 17. Surface motion of a point on the membrane over
narrow air gap as function of time.
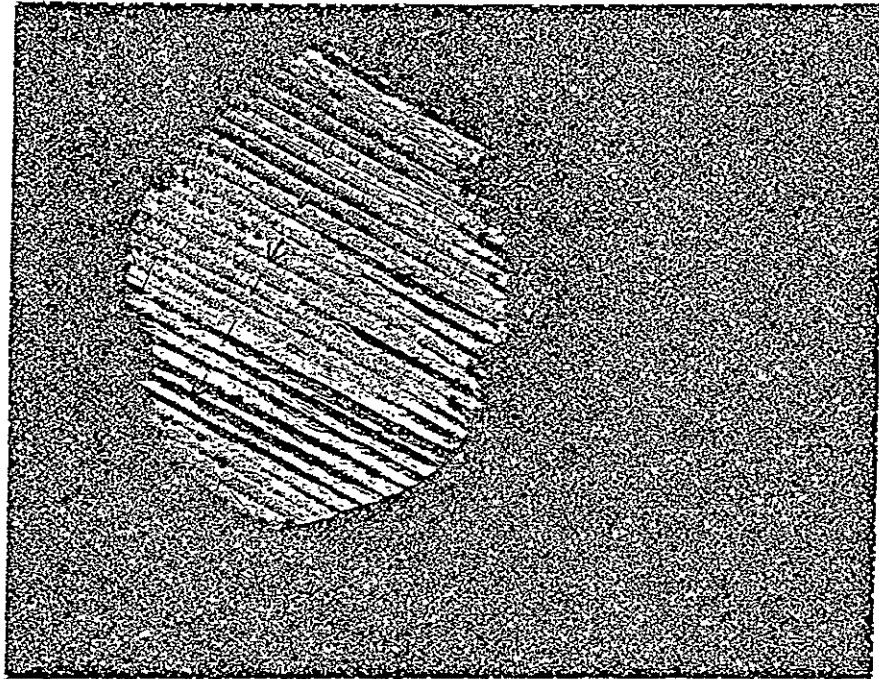
Figure 18. Area photograph of the surface motion of a
"dulcimer" model.
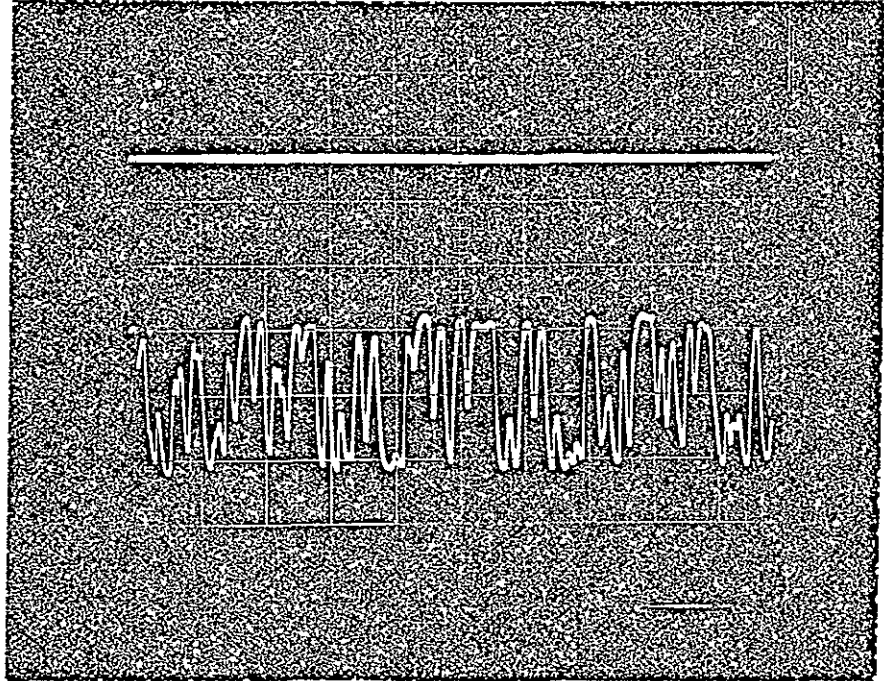
Figure 19. Surface response with time for the dulcimer model.

48

CONCLUSIONS

Theoretical analyses for common compliant wall geometries are presented. Analyses of surface motion for the compliant experiments indicate that the original Kramer experiments conducted in water could have interrupted the turbulent burst mechanism and produced the drag reduction. Membranes over thin air gaps can also be used to produce the small wavelength, large frequency motion required for air experiments. It is possible that in some laminated surface compliant wall experiments, delamination of the structure occurred and thereby created a narrow air gap situation; thus the observed drag reduction in the experiment of Walters (ref. 4) and the Langley experiment (ref. 5). The membranes over large air gaps do not show any promise at all. The "observed" drag reduction reported in reference 3 can be due to other effects, as suggested in reference 16. It seems rather difficult to obtain using passive walls the desired surface motion for most low speed and transonic speed experiments in air. Thus it may well be worthwhile to use active walls, i.e., walls where the motion is driven onto the surface for compliant experiments. Finally, there is a clear need to understand the entire fabric of fluid structural interaction, and this can only be achieved by bringing in and coalescing structural expertise with the fluid mechanics of turbulence. We believe that this report goes as far as making a first tentative step in the right direction toward such a goal.

APPENDIX A

FILM MATERIAL TESTS

By

Todd Hodges[1]

INTRODUCTION

Tests have been completed on eight materials in film form to support the compliant skin drag reduction project in the Fluid Mechanics Branch. The Fluid Mechanics Branch was interested in the elastic modulus of the materials they were using in their wind tunnel models.

TEST EQUIPMENT AND MATERIALS

Tests were conducted on the Eustron model TT-C located in room 003 of building 1293A. The C range load cell was used. Depending on the material being tested, the full scale ranges used were 1 lb, 2 lb, and 5 lb. Accuracy of the load cell is equal to, or exceeds, 0.25 percent of the range in use or 0.50 percent of the indicated load, whichever is greater. The amplifier and recorder accuracy is within 0.50 percent of full scale range.

Eustron air grips were used to hold the test specimens. Test gage length was 3 inches, and specimen width was 1/2 inch. Film thickness was measured by a power-driven film micrometer (Model 549E by Testing Machines, Inc.).

The test specimens were mounted and pulled at a constant crosshead speed of 1/2 inch per minute. The tensile modulus (E - psi) was calculated according to the attached equation derivation with an electronic calculator. Five samples were used on each test run except for the Latex rubber, where only three samples survived the film cutter.

---

[1] Research Associate, Virginia Polytechnic Institute and State University, Blacksburg, VA.

DISCUSSION

The following modulus values were measured on the eight systems:

1. Ethylene vinyl acetate copolymer (Alathon) (tested in the longitudinal direction). $E_{average}$ = 20.0 × 10^3 psi with a high of 20.6 × 10^3 psi and a low of 19.8 × 10^3 psi. This material showed good consistency in thickness and modulus.

2. Alathon (tested in the transverse direction). $E_{average}$ = 15.5 × 10^3 psi with a high of 16.5 × 10^3 psi and a low of 13.1 × 10^3 psi, also showed good consistency in thickness but not as good in modulus.

3. Latex rubber, $E_{average}$ = 296 psi, high 313 psi, low 272 psi. Lowest modulus of all the materials. We were able to salvage three test samples from the film-cutting device.

4. Aluminized kapton, $E_{average}$ = 416 × 10^3 psi, high 468 × 10^3 psi, low 390 × 10^3 psi. Modulus consistency was not good.

5. Aluminized P.B.C, $E_{average}$ = 361 × 10^3 psi, high 416 × 10^3 psi, low 296 × 10^3 psi. Thickness and modulus variation were high.

6. P.V.C., $E_{average}$ = 33.4 × 10^3 psi, high 36.9 × 10^3 psi, low 28.2 × 10^3 psi. Thickness and modulus variation were high.

7. Polyethylene, $E_{average}$ = 2.17 × 10^3 psi, high 22.8 × 10^3 psi, low 20.8 × 10^3 psi. Thickness and modulus consistency were good.

8. Aluminized mylar, $E_{average}$ = 451 × 10^3 psi, high 536 × 10^3 psi, low 367 × 10^3 psi. Thickness and modulus consistency were not good.

The aluminized films generally showed less consistency in thickness and modulus than plain films. This could be due to the coating technique they use and its effect on the substrate film.

Ranking the materials in order of modulus we have:

1. Latex rubber: E_{av} = 296 psi.
2. Alathon (transverse): E_{av} = 15.5 × 10^3 psi
3. Alathon (longitudinal): E_{av} = 20.0 × 10^3 psi
4. Polyethylene: E_{av} = 21.7 × 10^3 psi

5. P.V.C.: $E_{av} = 33.4 \times 10^3$ psi

6. Aluminized P.V.C.: $E_{av} = 361 \times 10^3$ psi

7. Alumnized kapton: $E_{av} = 390 \times 10^3$ psi

8. Aluminized mylar: $E_{av} = 451 \times 10^3$ psi.

VACUUM SUCTION TECHNIQUE FOR TENSIONING COMPLIANT MEMBRANES

In this section we shall briefly discuss the vacuum suction technique for tensioning the compliant membranes. The cross section of the vacuum suction chamber is shown in figure B-1. The shaded area of $(L_x \times L_y)$ is the
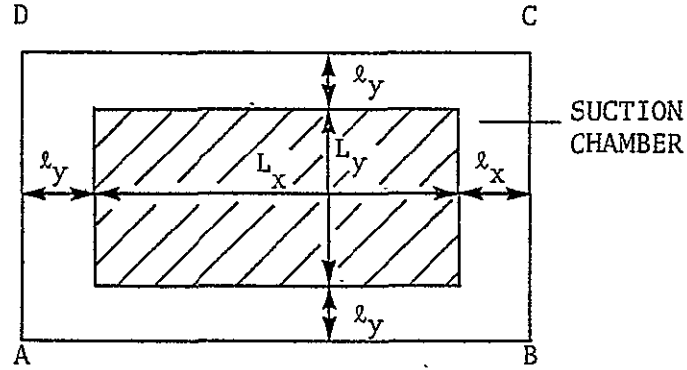
Figure B1.

working area of the model on which a uniform tension needs to be applied. In order to apply uniform tension in the working model the width of the cavities ℓ_x, ℓ_y have to be related in some fashion to the dimensions L_x, L_y.

Initially the membrane is taped to the sides ABCD with care such that there is little tension on the membrane. The suction chamber pressure is at ambient pressure during this time. Now the chamber pressure is adjusted to be lower than the ambient pressure by a magnitude Δp. The deflections of the membrane at the center of the channels w_1, w_2 are noted.

In figure B-2 we indicate schematically what happens to a cross section of the membrane. For the simply supported membrane of length ℓ_x and width $(L_y + 2\ell_y)$ where the ratio $\left(\dfrac{\ell_x}{L_y + 2\ell_y} \right) \ll 1$ we can approximate the governing equation as:
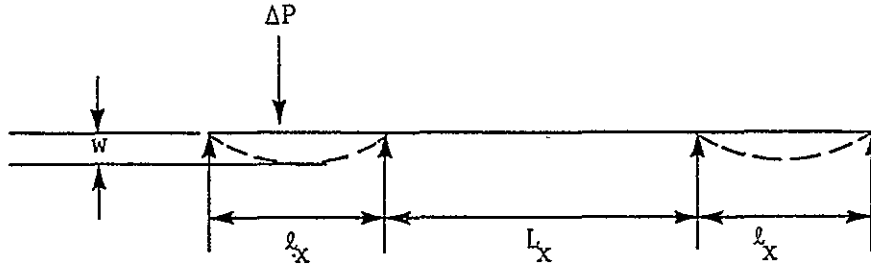
$$T \frac{\partial^2 w}{\partial x^2} = \Delta p \tag{B-1}$$

$$w(0) = w(\ell_x) = 0 \tag{B-2}$$

Assuming

$$w = \sum W_m \sin \frac{m\pi x}{\ell_x} \tag{B-3}$$

one obtains for W_m, after substituting in equation (B-1)

$$W_m = \frac{2\Delta p}{(m\pi)^3} \frac{\left(1 - (-1)^m\right)}{T} \ell_x^2 \tag{B-4}$$

Thus all odd modes are present in the solution and

$$w_1 = \sum_{m=1}^{\infty} W_m \sin \frac{m\pi x}{\ell_x} = \frac{4\Delta p \ell_x^2}{\pi^3 T} \sum_{m=1,3,5\ldots\infty} \left(\sin \frac{m\pi x}{\ell_x}\right) \frac{1}{m^3}$$

$$\simeq (0.125) \left(\frac{\ell_x^2}{T_x}\right) \Delta p \tag{B-5}$$

54

Similarly,

$$w_2 = 0.125 \left(\frac{\ell_y^2}{T_y}\right) \Delta p \tag{B-6}$$

Thus

$$\frac{w_1}{w_2} = \left(\frac{\ell_x}{\ell_y}\right)^2 \left(\frac{T_y}{T_x}\right) \tag{B-7}$$

Now, the stretching that the membrane undergoes in the cavity ℓ_x is contributed by the stretching of the membrane in the working area. The stretching in the cavity ℓ_x is given by

$$\Delta \ell = \int_o^{\ell_x} \sqrt{1 + \left(\frac{\partial w}{\partial x}\right)^2} \; dx - \ell$$

$$= \frac{1}{2} \int_o^{\ell_x} \left(\frac{\partial w}{\partial x}\right)^2 dx$$

$$= \frac{1}{2} \frac{\ell_x}{2} \left[\frac{16\Delta p^2 \ell_x^2}{\pi 4 T_x^2}\right] \sum \frac{1}{m^4}$$

$$= 0.0417 \Delta p^2 \left(\frac{\ell_x^3}{T_x^2}\right) \tag{B-8}$$

The stretching $\Delta \ell$ is assumed to be caused by a uniform loading P per unit width applied to the membrane of the working area of the model, in which case

$$\frac{PL_x}{Eh} = \Delta \ell = 0.0417 \Delta p^2 \left(\frac{\ell_x^3}{T_x^2}\right)$$

or

$$P = \left(\frac{\ell_x^3}{L_x}\right) \quad 0.0417\left(\frac{Eh\Delta p^2}{T_x^2}\right) \tag{B-9}$$

Similarly the loading P_1 on the end in the y direction is

$$P_1 = \left(\frac{\ell_y^3}{L_y}\right) \quad 0.0417\left(\frac{Eh\Delta p^2}{T_y^2}\right) \tag{B-10}$$

Finally, we would expect to have $P = P_1$ and $T_x = T_y$ for uniform tensioning when

$$\left(\frac{\ell_x}{\ell_y}\right) = \left(\frac{L_x}{L_x}\right)^{1/3} \tag{B-11}$$

which is as given in equation (72).

APPENDIX C

CODE FOR ANALYZING MEMBRANE WITH BACKING,

OR WITH CAVITIES BEHIND IT

```
      PROGRAM MAIN(INPUT,OUTPUT,TAPE5=INPUT,TAPE6=OUTPUT)

      COMPLEX DU,X2,X3

      DIMENSION AK(75,24),AFACT(75),BFACT(24)

      DIMENSION W1(5500)

      DIMENSION OMC(75,24),CM1(75,24)

      DIMENSION FF(80)

C****************************************************************************
C
C
C
C        THIS PROGRAM EVALUATES THE RESPONSE OF A MEMBRANE WITH DEEP
     1    CAVITY(AIR), A MEMBRANE WITH WATER BACKING, AND  AMEMBRANE
     2 ON ELASTIC FOUNDATION
     1    CAVITY(AIR), AMEBRANE
C        BULL-S SPECTRUM IS USED TO OBTAIN THE EXCITATION FIELD
C**        INDUCED AERODYNAMIC EFFECTS   USING PISTON THEORY.
C**     EFFECTS OF BACKING USING POTENTIAL FLOW THEORY.
C**  THEORETICAL MODEL USES LINEAR THEORY
C**        PROPER VALUES OF DAMPING INCLUDED USING LAB ESTIMATES
C             OUTPUT---FREQUENCY,MEAN SQUARE FORCING FUNCTION ,MEAN SQ
     1UARE RESPONSE FUNCTION, MEANSQARE AMPLITUDE.
C     ALL DATA TO BE IN IN-LB-SEC UNITS
```

```
C
C
C
C*************************************************************************
      NR=5$NW=6$G=386.0$EPS=0.000000001$CO=1.35*10.**4$PI=3.1415926

      DO 110 J=1,5

      READ(NR,111)(FF(I),I=1,80)

  111 FORMAT(80A1)

  110 CONTINUE

      WRITE(NW,888)

  888 FORMAT(//5X,*CASE1 WTR BCK MEM,C 52 MEM DP CAV,C53MEM PLAS*)

      DO 777 IJKL=1,3

      READ(NR,101)A,B,T,EM1,ETA,DELT,UREF,U,RHO1,RHO2,H

  101 FORMAT(8F10.5)

      READ(NR,102)IJK,AKF

  102 FORMAT(I1,F14.6)

      EM1=EM1*(.1)**7$RHO1=RHO1/(12.)**4$RHO2=RHO2/(12.)**4

      DSTAR=7./72.*DELT

      DO 5 L=1,75

      AL1=(L-1)*2.+1.

      DO 5 N=1,24

      AN1=(N-1.)*2.+1.

      AK1=(AL1*PI/A)**2+(AN1*PI/B)**2
```

```
      OMC(L,N)=CO*SQRT(AK1)

      AK(L,N)=AK1

5     CONTINUE

      DO 6 L=1,75,2

      OMCUT=OMC(1,1)-5.

6     AFACT(L)=1.0

      DO 7 L=2,74,2

7     AFACT(L)=-1.0

      DO 8 N=1,24,2

8     BFACT(N)=1.0

      DO 9 N=2,24,2

9     BFACT(N)=-1.0

      WRITE(NW,801)U

801   FORMAT(//20X,F15.6)

      DST1=DSTAR

      Q=0.5*RHO1*U**2

      CONST=Q**2*DST1/U*1.

      CONST1=0.0064516

      CON1=DST1/U

      UC=0.8*U

802   FORMAT(//20X,*LOWER CUTOFF FREQ.,(BULL)*,F15.6,*UPPER CUTOFF*,F15.

     16)

      W=0.0
```

```
      JK=0

      DOM=1.0$OM2=2.*PI*DOM

      OMEG=0.05/CON1

      EE1=EXP(0.1)$EE2=EXP(0.0235)$EE3=EXP(0.40)

      DO 2 J=1,5

      OM3=OM2

      OM2=OM3*10.

      DO 31=1,90

      JK=JK+1

      AI=I

      OM1=OM3*(1.+AI/10.)

      OML=0.1*OM3

      F=OM1/2./PI

      OMC1=250.*1./CON1*2.*PI

      OMCC=OMC1/10.

      IF(OM1.GT.OMCC)GO TO 28

      IF(OM1.GT.OMC1) GO TO 31

      IF(OM1.LE.OMEG)GO TO 23

      ATOM=8.*OM1*CON1

      TWOM=2.*OM1*CON1

      FRACOM=0.47*OM1*CON1

      IF(ATOM-12.)12,13,13

   12 E1=1./EXP(ATOM)
```

```
        GO TO 14

13   E1=0.0

14   CONTINUE

     IF(TWOM-12.)15,16,16

15   E2=1./EXP(TWOM)

     GO TO 17

16   E2=0.0

17   CONTINUE

     IF(FRACOM-12.)18,19,19

18   E3=1./EXP(FRACOM)

     GO TO 20

19   E3=0.0

20   CONTINUE

     E=E2*3.7+0.8*E3-3.4*E1

     GO TO 22

28   E=3.15/225.0

     GO TO 22

31   E=0.0

     GO TO 22

23   E=(OMI/OMEG)**4*(3.7/EE1-3.4/EE3+0.8/EE2)

22   CONTINUE

     FORE=CONST*E

803  FORMAT(//20X,*FORCING FIELD--AMP.=*,F15.6,*FREQ.=*,F15.6)
```

```
      BK=OM1/UC$BK1=1.+COS(BK*A)$BK2=SIN(BK*A)

      DU=CMPLX(0.0,0.0)

      ETA1=ETA*OM1

      OMN=(OM1/CO)**2

      XX=PI/A$XXX=XX**2$ASQ=A**2$BKSQ=BK**2

      IF(IJK.EQ.1)RHO2=0.0

      DO 10 L=1,75

      AL=(L-1.)*2.+1.

      AL1=AL*XX

      APL=ABS(AL1-BK)

      IF(APL.LE.EPS)GO TO 51

      ALX1=(AL1**2-BKSQ)*ASQ

      D11=BK1*8.*AL*AFACT(L)/ALX1

      D12=D11*BK2/BK1

      GO TO 52

51    D11=0.

      D12=-4./PI*AFACT(L)

52    CONTINUE

      DO 10 N=1,24

      AN=(N-1.)*2.+1.

      X11=D11/AN*BFACT(N)

      X12=D12/AN*BFACT(N)

      X3=CMPLX(X11,X12)
```

```
      AK1=AK(L,N)-OMN

      IF(OM1.LT.OMCUT)GO TO 93

      IF(ABS(AK1).LE.EPS)GO TO 92

      IF(AK1-EPS)91,92,93

91    AK2=-AK1

      AK2=SQRT(AK2)*H

      CT=COS(AK2)/SIN(AK2)

      X1=-(EM1+RHO2*H*CT/AK2)*OM1**2+AK(L,N)*T+RHO2*G

      X1=X1+AKF

      X5=ETA1+OM1**2*RHO1*H*1./AK2

      X2=CMPLX(X1,X5)

      GO TO 97

93    AK2=SQRT(AK1)*H*2.

      CX=EXP(AK2)

      CTH=(CX+1.)/(CX-1.)

      X1=-((RHO1+RHO2*CTH)*2.*H/AK2+EM1)*OM1**2+AK(L,N)*T+G*RHO2

      X1=X1+AKF

      X2=CMPLX(X1,ETA1)

97    CONTINUE

      CM1(L,N)=CABS(X3/X2)

      DU=X3/X2+DU

92    CONTINUE

10    CONTINUE
```

```
987 FORMAT(15E8.2)

    W1(JK)=CABS(DU)**2

    W1(JK+1000)=W1(JK)*FORE

    W1(JK+1000)=CONST1*W1(JK+1000)

    W=W+W1(JK+1000)*OML

    WRITE(NW,909)F,FORE,W1(JK),W1(JK+1000),W

909   FORMAT(5X,5E20.7)

3     CONTINUE

2     CONTINUE

1     CONTINUE

777 CONTINUE

    STOP

    END

_

C        GIVE EM1=EM1*10.**7$RHOS =RHO*144.**2

DATA TO BE FED ARE LENGTH OF MODEL(A),WIDTH OF MODEL(B),TENSION OF MEMBRANE(T)

MASS OF MEMBRANE(EM1),DAMPING(VISCOUS) COEFFICIENT(ETA),BOUND.LAYER THKNSS(DELT)

,REF.VEL(UREF),VELOCITY(U),DENSITY FLD1(RHO1),DENS.FLD2(RHO2)HT OF CAVITY(H)

FORMAT NUMBER IS   101  ,8F10.4

26.0       8.0        0.02       1.1        0.0002     0.6        636.0      636.0

0.00234    1.9379     0.5


50.0       18.0       1.0        1.1        0.0002     1.6063     1318.9     1318.9
```

0.00234   0.00234   0.08

50.0   18.0   1.0   .1.1   0.0002   1.6063   1318.9   1318.9

0.00234   0.00234   0.08

10.666666

APPENDIX D

CODE FOR ANALYZING PERIODIC STRUCTURE RESPONSE

```
      PROGRAM KRAMER(INPUT,OUTPUT,TAPE5=INPUT,TAPE6=OUTPUT,TAPE1)

C*****************R********************************************************************

C**

C          THIS PROGRAM  EVALUATES THE MEAN SQUARE RESPONSE OF A KRAMER

    1 PERIODIC SURFACE. THE SURFACE IS A RUBBER DIAPHRAGM SUPPORTED

    2 PERIODICALLY(80 MIL APART) BY RUBBER STUBS AND FILLED WITHBWATER.

C**          INDUCED AERODYNAMIC EFFECTS  USING PISTON THEORY.

C**          EFFECTS OF BACKING USING POTENTIAL FLOW THEORY.

C**   THEORETICAL MODEL USES LINEAR THEORY

C**          PROPER VALUES OF DAMPING INCLUDED USING LAB ESTIMATES

C          ANALYSIS --SEE SECTION 6.

C          ALL UNITS LB-SEC-FT

C          BULLS SPECTRUM FOR EXCITING FIELD

C**

C*****************R********************************************************************

      DIMENSION A(21),B(21),C(21),D(21),IJ(21),          FORE(12000),W(15),

    1ASUM(15)

      DIMENSION GE(21),F(21)

      DIMENSION HEF(21)

      NR=5$NW=6

C     DATA

      H=0.040$RHO=62.4$G=386.$U=720.$ETA=0.001$E=2000.$EM1=8.8$ANU=0.45
```

```
      DELTA=1.08$Y=0.$TPI=6.2831852604CO=57000.

      ETA=0.0000001

      EPS=0.00000001

C         INITIALISATION OF DATA

      EM1=EM1*(.1)**6$RHO=RHO/32.2/12./12./12./12.$DST1=7./72.*DELTA

      AKF=E$A1=H/AKF$P1=A1

      AKF=20.0$A1=H/AKF$P1=A1

      EM1=EM1*A1

      DD=E*H**3/3./(1.-ANU**2)

      D1=DD*A1$ETA1=ETA*A1$UC=0.8*U$Q=0.5*RHO*U**2$CON1=DST1/U$Q1=Q**2*C
   1ON1

      G1=G*RHO*A1

      OMEG=0.05/CON1$DOM=0.1*TPI$OM2=DOM

      DOM=10.*TPI

      OM2=DOM

      OMC1=25.*TPI*U/DELTA

      OMCC=10.*OMC1

C         INITIALISE ARRAYS

      DO 101 J=1.15

      ASUM(J)=0$W(J)=0.

  101 CONTINUE

C         MAJOR LOOP FOR INCRENENT OF OM

      JJ=0$EE1=EXP(0.10)$EE2=EXP(0.0235)$EE3=EXP(0.40)
```

```
C       DO 2 JK=1,6

        OM3=OM2$OM2=OM3*10.

C       DO 1  JL=1,90

        DO 1  JL=1,20000

        AJ=JL

        OM1=OM3*(1.+AJ/10.)

        FF=OM1/TPI

        JJ=JJ+1

        UC=0.8*U

        IF(OM1.LE.OMEG)GO TO 23

        IF(OM1.GE.OMC1)GO TO 511

        IF(OM1.GT.OMCC)GO TO 513

        ATOM=8.0*OM1*CON1

        TWOM=2.*OM1*CON1

        FRACOM=0.47*OM1*CON1

        IF(ATOM-60.)12,13,13

   12   E1=1./EXP(ATOM)

        GO TO 14

   13   E1=0.

   14   CONTINUE

        IF(TWOM-60.)15,16,16

   15   E2=1./EXP(TWOM)

        GO TO 17
```

```
16   E2=0.0

17   CONTINUE

     IF(FRACOM-60.)18,19,19

18   E3=1./EXP(FRACOM)

     GO TO 20

19   E3=0.

20   CONTINUE

     E=E2*3.7+0.8*E3-3.4*E1

     GO TO 22

511  E=3.18/225.

     UC=0.39*U

     GO TO 22

513  STOP

23   E=3.7/EE1+0.8/EE2-3.4/EE3

     E=E*(OM1/OMEG)**4

22   CONTINUE

     FORE(JJ)=Q1*E*0.00001

     AK1=(OM1/CO)**2$AMU=OM1/UC*H$ETAI=ETAI*OM1

     M=-11$SUM=0.$SUM1=0.

     DO 30  M1=1,21

     M=M1-11

     AM1=M

     AML=(AMU+AM1*TPI)/H
```

```
      AK=AML**2-AK1

      A(M1)=D1*AML**4+G1-OM1**2*EM1$B(M1)=ETAI

      IF(ABS(AK).LE.EPS)GO TO 40

      IF(AK-EPS)39,40,41

40    IJ(M1)=1

      GO TO 47

39    CONTINUE

      IJ(M1)=0

      AK=-AK

      AK=SQRT(AK)

      SK=AK*H

      S1=SIN(SK)$C1=COS(SK)

      IF(S1.EQ.0)   GO TO 901

      A(M1)=A(M1)+RHO*A1*C1/S1/AK*OM1**2$B(M1)=B(M1)+RHO*A1/AK*OM1**2

      GO TO 902

901   IJ(M1)=1

902   CONTINUE

      GO TO 47

41    IJ(M1)=0

      AK=SQRT(AK)

      SK=AK*2.*H

      SK1=EXP(SK)

      CTH=(SK1+1.)/(SK1-1.)
```

```
52    CONTINUE

      A(M1)=A(M1)-OM1**2*RHO/AK*A1*(1.+CTH)

47    CONTINUE

      IF(IJ(M1))48,48,49

48    CONTINUE

      A2=A(M1)**2+B(M1)**2

      SUM=SUM+A(M1)/A2

      SUM1=SUM1+B(M1)/A2

49    CONTINUE

30    CONTINUE

      A9=A(11)**2+B(11)**2

      GAM1=A1*(A(11)*(SUM+1.)+B(11)*SUM1)

      GAM1=GAM1/A9/((1.+SUM)**2+SUM1**2)

      GAM2=A1/A9*(A(11)*SUM1-B(11)*(SUM+1.))/(SUM1**2+(1.+SUM)**2)

      DO 60 M1=1,21

      IF(IJ(M1))61,62,61

61    CONTINUE

      D(M1)=0.0

      C(M1)=0.0

      GO TO 67

62    CONTINUE

      C(M1)=(A(M1)*GAM1+B(M1)*GAM2)/(A(M1)**2+B(M1)**2)

      D(M1)=(B(M1)*GAM1-A(M1)*GAM2)/(A(M1)**2+B(M1)**2)
```

```
92   CONTINUE
     WRITE(NW,200)FF,ASUM(4),GE(11),GE(12),GE(10),HEF(11),HEF(12),HEF(1
    10),W(4),FORE(JJ)
603   FORMAT(/50X,*IM*)
209 FORMAT(1X,10E12.5)
208 FORMAT(//5X,10E12.6)
1     CONTINUE
2     CONTINUE
201 FORMAT(1X,7E16.7)
     STOP
     END
```

APPENDIX E

CODE FOR ANALYZING MEMBRANE UNDER NARROW AIR GAP

.

```
RUN(S)

REQUEST,TAPE1,HY.          SAVTP,RIL,RSB,TW20.

REWIND(TAPE1)

-

        PROGRAM   MEMGAP(INPUT,OUTPUT,TAPE5=INPUT,TAPE6=OUTPUT,TAPE1)

        DIMENSION W(51,51),WO(51,51),WN(51,51),P(51,51),AU(101)

C       T=TENSION (LBF/IN)

C       RHO=MEMBRANE DENSITY (LBM/CU.FT)

C       E=SUBSTRATE MODULUS OF ELASTICITY (PSI)

C       D=SUBSTRATE DEPTH (IN)

C       GAP=GAP BETWEEN MEMBRANE AND SUBSTRATE (IN)

C       H=MEMBRANE THICKNESS (IN)

C       B=DAMPING COEFFICIENT (LBF-SEC/CU.FT)

C       DX=ELEMENT SIZE (IN)

C       NI=NUMBER OF NODES IN X-DIRECTION

C       NJ=NUMBER OF NODES IN Y-DIRECTION

C       NT=NUMBER OF TIME STEPS--DT=DX/C WHERE C IS WAVE SPEED

C          GM IS TIME STEP CONTROL---  DT=DX/(C*GM)

        T=1

        RHO=87

        E=1.

        D=0.25
```

```
          NW=6

          H=0.001

          B=0.000001

          NI=51$NJ=51$DX=0.2

          U=50$DELTA=1.$PI=3.1415926

          NT=20000

          PMAX=0.00234*U**2*0.5*0.01

          P1=PMAX*U**2/DX**2

          P1=P1*144.

          F=1.2*U*12./P1/2./DELTA

C         CONVERT INPUT TO CONSISTENT UNITS

          T=12.*T

          RHO=RHO/32.174

          E=144.*E

          D=D/12

          GAP=GAP/12.

          H=H/12.

C         WAVE SPEED IS GIVEN BY SQ. RT. OF T/(RHO*H)

          C=(T/(RHO*H))**0.5

          DX=DX/12

          DT=5*0.1**6

          GM=DX/C/DT
```

```
C        INITIALIZE DISPLACEMENTS

         DO 2 I=1,NI

         DO 1 J=1,NJ

         WO(I,J)=0.

         W(I,J)=0.

         WN(I,J)=0.

         P(I,J)=0.

    1 CONTINUE

    2 CONTINUE

         B=B*C

C        CALCULATE NEW DISPLACEMENTS

C        PRESSURE LOADING CAN BE ENTERED HERE

         IT=2

         NIX=NI-1

         NJY=NJ-1

         A1=B*GM/(2.*T*DX)+(GM/DX)**2

         A2=1./DX*1./DX

         A3=B*GM/(2.*T*DX)-(GM/DX)**2

         A4=F/(D*T)

         A5=1./T

         TE=1./F$OM=2.*PI*F$T1=DX/U$TWOT1=2.*T1

         TPLT1=TE+T1

         TPLT2=TE+TWOT1
```

```
      ENI=NI-1
      TMAX=ENI/(XDX+1.)/(+DX/U
      REWIND 1
      DO 130 N=1,NT
      IT=2+N
      TIME=N*DT
      T=TIME
      DO 227 IX=2,NI
      DO 227 JY=2,NJ
  227 P(IX,JY)=0.0
      IF(TIME-TMAX)201,210,210
  201 DO 209 IX=2,NIX
      EXX=IX-2
      T=TIME-EXX*DX/U
      IF(T)152,152,154
  154 IF(T-T1)155,155,151
  155 CONTINUE
      DO 221 JY=2,NJY
  221 P(IX,JY)=P1*(T/OM-SIN(OM*T)/OM**2)
      GO TO 152
  151 IF(T-TWOT1)156,156,157
  156 CONTINUE
      DO 222 JY=2,NJY
```

```
222 P(IX,JY)=P1*(TWOT1/OM-T/OM+2.*SIN(OM*(T-T1))/OM**2-SIN(OM*T)/OM**2
   1)
     GO TO 152
157 IF(T-TE)158,158,159
158 CONTINUE
     DO 223 JY=2,NJY
223 P(IX,JY)=P1*2./OM**2*SIN(OM*(T-T1))*(1.-COS(OM*T1))
     GO TO 152
159 IF(T-TPLT1)160,160,161
160 CONTINUE
     DO 224. JY=2,NJY
224 P(IX,JY)=P1*((T-T1)/OM+2./OM**2*SIN(OM*(T-T1))-SIN(OM*(T-TWOT1))/O
   1M**2)
     GO TO 152
161 IF(T-TPLT2)162,162,152
162 CONTINUE
     DO 225 JY=2,NJY
225 P(IX,JY)=P1*((T-TE-TWOT1)/OM-SIN(OM*(T-TWOT1))/OM**2)
152 CONTINUE   .
209 CONTINUE
210 CONTINUE
     DO 20 I=2,NIX
     DO 10 J=2,NJY
```

```
      SUM=W(I+1,J)+W(I-1,J)+W(I,J+1)+W(I,J-1)

      SUM=SUM+(2.*GM**2-4.)*W(I,J)

      SUM1=WO(I,J)

      SUM2=A4*(W(I,J)+GAP)

      WN(I,J)=SUM*A2/A1+SUM1*A3/A1-P(I,J)*A5/A1

      IF(W(I,J)+GAP)5,5,6

5     WN(I,J)=2.*WO(I,J)-W(I,J)

6     CONTINUE

10    CONTINUE

20    CONTINUE

      AI=NI-1

      BI=100.

      DEL=BI/AI

      IDEL=DEL +0.2

      DO 19 I=1,101

      EI=I-1

      J=(I-1)/IDEL+1

      EJ=J-1

      J1=J+1

      XI=EI/DEL-EJ

      AU(I)=WN(J,11)*(1.-XI)+WN(J1,11)*XI

19    CONTINUE

      WRITE(1)AU
```

```
C        SHIFT LOCATIONS OF W ARRAYS
         DO 91  I=2,NIX
         DO 91  J=2,NJY
         WO(I,J)=W(I,J)
         W(I,J)=WN(I,J)
91       CONTINUE
130      CONTINUE
         STOP
         END
```

REFERENCES

1. Ash, R.L; Bushnell, D.M.; Weinstein, L.M.; and Balasubramanian, R.: Compliant Wall Surface Motion and Its Effect on the Structure of a Turbulent Boundary Layer. Fourth Biennial Symposium on Turbulence in Liquids, Sep 1975, University of Missouri, Rolla.

2. Kramer, M.O.: Boundary Layer Stabilization by Distributed Damping. ASNE Journal, Feb 1960, pp. 25-34.

3. Looney, W.R. and Blick, E.F.: Skin Friction Coefficient of Compliant Surfaces in Turbulent Flow. J. Spacecraft, 1966, vol. 3, no. 10, pp. 1562-1564.

4. Walters, R.R.: Turbulent Boundary Layer Characteristics of Flow Over a Compliant Surface. Ph.D. thesis, University of Oklahoma, 1969.

5. Fischer, M.C.; Weinstein, L.M.; Bushnell, D.M.; and Ash, R.L.: Compliant Wall Turbulent Skin Friction Reduction Research. AIAA Paper No. 75-833, Eighth Fluid and Plasma Dynamics Conference, Jun 1975, Hartford, CT.

6. Orszag, S.A.: Private communications. Also see Proceedings of Compliant Wall Drag Reduction Contractor Meeting, Jan 1977, Langley Research Center, Hampton, VA.

7. Collins, Don and Kendall, J.M. Private communications. Also see Proceedings of Compliant Wall Drag Reduction Contractor Meeting, Jan 1977, Langley Research Center, Hampton, VA.

8. Gyorgyfalvy, D.: The Possibilities of Drag Reduction by the Use of Flexible Skin. AIAA Paper No. 66-430, Fourth Aerospace Sciences Meeting, Jun 1966, Los Angeles, CA.

9. Kaplan, R.E.: The Stability of Laminar Incompressible Boundary Layers in the Presence of Compliant Boundaries. ASRL TR 116-1, Jun 1964, Massachusetts Institute of Technology, Cambridge, MA.

10. Tokita, N. and Boggs, F.W.: Final Report on Theoretical Study of Compliant Coatings to Achieve Drag Reduction on Underwater Vehicles. U.S. Rubber Company, Research and Development Department, Research Center, Wayne, NJ, March 1962.

11. Burden, H.W.: The Effect of Wall Porosity on the Stability of Parallel
     Flows Over Compliant Boundaries. Ph.D. thesis, University of Pennsylvania,
     1969.

12. Bull, M.K.: Wall Pressure Fluctuations Associated With Subsonic Turbu-
     lent Boundary Layer Flows. J. Fluid Mech., vol. 28, no. 67, pp. 719-
     754.

13. Karman, Th. von and Lin, C.C.: Advances in Applied Mechanics, vol. 2,
     no. 1, 1951.

14. Ash, R.L.: Simulation of Turbulent Wall Pressure. Old Dominion Univer-
     sity School of Engineering Technical Report 76-T2, Norfolk, VA, March
     1976.

15. Mead, D.J. and Pujara, K,K.: Space Harmonic Analysis of Periodically
     Supported Beams: Response to Convected Random Loading. J. Sound and
     Vibration, vol. 14, no. 4, pp. 525-541, 1971.

16. Hefner, J.N. and Weinstein, L.M.: Reexamination of Compliant Wall
     Experiments in Air with Water Substrates. J. Spacecraft and Rockets,
     Vol. 13, no. 8, pp. 502-503, Aug 1976.

17. Bushnell, D.M.; Hefner, J.N.; and Ash, R.L.: Compliant Wall Drag
     Reduction for Turbulent Boundary Layers. IUTAM Symposium on Structure
     of Turbulence and Drag Reduction, Jun 1976, Washington, DC.